

NPS-53-89-012

# NAVAL POSTGRADUATE SCHOOL

## Monterey, California

2

AD-A205 578



RAYLEIGH-TAYLOR INSTABILITY OF A VISCOUS FILM  
OVERLYING A PASSIVE FLUID

David Canright  
Stephen Morris

February 1989

Approved for public release; distribution unlimited  
Prepared for:

Naval Postgraduate School and  
National Science Foundation,  
Washington, D.C. 20550

DTIC  
ELECTE  
S 21 MAR 1989 D  
E

89

2

21

002


NAVAL POSTGRADUATE SCHOOL  
Department of Mathematics

Rear Admiral R. C. Austin  
Superintendent

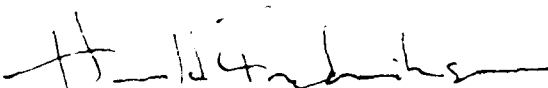
Harrison Shull  
Provost

This report was prepared in conjunction with research conducted for the National Science Foundation and for the Naval Postgraduate School and funded by the Naval Postgraduate School Research Council. Reproduction of all or part of this report is authorized.


Prepared by:

  
DAVID CANRIGHT  
Adjunct Professor of Mathematics

Reviewed by:

  
HAROLD M. FREDRICKSEN  
Chairman  
Department of Mathematics

Released by:

  
KNEALE T. MARSHALL  
Dean of Information  
and Policy Sciences

REPORT DOCUMENTATION PAGE				
1a REPORT SECURITY CLASSIFICATION UNCLASSIFIED		10 RESTRICTIVE MARKINGS		
14 SECURITY CLASSIFICATION AUTHORITY		1 DISTRIBUTION/AVAILABILITY OF REPORT Approved for public release; distribution unlimited		
16 DECLASSIFICATION/DOWNGRADING SCHEDULE		5 MONITORING ORGANIZATION REPORT NUMBER(S) NPS-53-89-012		
4 PERFORMING ORGANIZATION REPORT NUMBER(S) NPS-53-89-012		14 NAME OF MONITORING ORGANIZATION Naval Postgraduate School and the National Science Foundation		
6a NAME OF PERFORMING ORGANIZATION Naval Postgraduate School	6b OFFICE SYMBOL (if applicable) 53	1b ADDRESS (City, State, and ZIP Code) Monterey, CA 93943 and Washington, D.C. 20550		
8a NAME OF FUNDING/SPONSORING ORGANIZATION Naval Postgraduate School	8b OFFICE SYMBOL (if applicable) 53	7 PROCUREMENT INSTRUMENT IDENTIFICATION NUMBER O&MN Direct funding		
8c ADDRESS (City, State, and ZIP Code) Monterey, CA 93943		10 SOURCE OF FUNDING NUMBERS		
		PROJECT ELEMENT NO	TASK NO.	22b TELEPHONE ACCESSION NO
11 TITLE (Include Security Classification) Rayleigh-Taylor Instability of a Viscous Film Overlying a Passive Fluid				
12 PERSONAL AUTHOR(S) David Canright and Stephen Morris				
13a TYPE OF REPORT Technical Report	13b TIME COVERED FROM 6/85 TO 4/87	14 DATE OF REPORT (Year, Month, Day) February 1989	15 PAGE COUNT 46	
16 SUPPLEMENTARY NOTATION				
17 COSAT CODES		18 SUBJECT TERMS (Continue on reverse if necessary and identify by block number)		
FIELD	GROUP	SUB GROUP	Rayleigh-Taylor instability mantle convection	
19 ABSTRACT (Continue on reverse if necessary and identify by block number)				
<p>To help understand the stability of cold, viscous boundary layers in geophysical contexts such as lava lakes and mantle convection, the following model problem is analyzed: Beneath a shear-free horizontal boundary, a thin layer of very viscous fluid overlies a deep layer of less viscous, less dense fluid. The initial unstable equilibrium is perturbed, and the growth of the disturbance is followed, including the nonlinear effects of large amplitude, by a long-wave analysis. The result shows that, in the final catastrophic growth, the peak thickness of the upper layer approaches infinity inversely proportional to the remaining time. (This conclusion also applies to fluids with power-law rheology.) Thus nonlinear effects greatly enhance growth. <i>Reminders: Earth and Space Science</i></p>				
20 DISTRIBUTION/AVAILABILITY OF ABSTRACT <input checked="" type="checkbox"/> UNCLASSIFIED/DISTRIBUTED <input type="checkbox"/> SAME AS RPT <input type="checkbox"/> OTIC USERS		21 ABSTRACT SECURITY CLASSIFICATION UNCLASSIFIED		
22a NAME OF RESPONSIBLE INDIVIDUAL David Canright		22b TELEPHONE (include Area Code) (408) 646-2782		22c OFFICE SYMBOL 53Ca

Rayleigh-Taylor instability of a viscous film  
overlying a passive fluid

David Canright  
Department of Mathematics  
Naval Postgraduate School  
Monterey, California, 93943

and

Stephen Morris  
Department of Mechanical Engineering  
University of California  
Berkeley, California, 94720

Accession For	
NTIS CPA&I	<input checked="checked" type="checkbox"/>
DTIC TAB	<input type="checkbox"/>
Unannounced	<input type="checkbox"/>
Justification	
By _____	
Distribution/ _____	
Availability Codes	
Dist	Avail and/or Special
A-1	

# ABSTRACT

To help understand the stability of cold, viscous boundary layers in geophysical contexts such as lava lakes and mantle convection, the following model problem is analyzed: Beneath a shear-free horizontal boundary, a thin layer of very viscous fluid overlies a deep layer of less viscous, less dense fluid. The initial unstable equilibrium is perturbed, and the growth of the disturbance is followed, including the nonlinear effects of large amplitude, by a long-wave analysis. The result shows that in the final catastrophic growth the peak thickness of the upper layer approaches infinity inversely proportional to the remaining time. (This conclusion also applies to fluids with power-law rheology.) Thus nonlinear effects greatly enhance growth.

1. Introduction	1
2. Problem Statement	3
3. Long-wave Analysis	5
4. Solutions	10
4.1. Localized Disturbance	10
4.2. Constant Wavelength Disturbance	12
4.3. Large-amplitude Behavior	13
5. Plume Formation	14
6. Conclusions	20
Appendices:	
A. Linearized Analysis	22
B. Power-law Fluid	26
C. Large-amplitude Similarity Solution	28
References	33

### Summary of notation

$\rho_1, \mu_1, \rho_2, \mu_2, \Delta\rho, g, x, z, t, u, w$  : see Figure 1

$\rho$  : local density ( $\rho_1$  or  $\rho_2$ )

$\nu$  : either kinematic viscosity

$k$  : characteristic wavenumber

$d_1, d_2$  : equilibrium depths of each layer

$\delta(x,y,t)$  : interface location

$P$  : local pressure ( $P_1$  or  $P_2$ )

$p$  : local reduced pressure (reduced by  $\rho g(z-d_1)$ )

$\underline{\underline{\sigma}}$  : stress tensor

$\tau_{ij}$  : deviatoric stress tensor (without pressure contribution)

$\alpha \equiv \mu_2/\mu_1$  : viscosity ratio

$\beta \equiv d_2/d_1$  : depth ratio

$\epsilon \equiv kd_1$  : dimensionless wavenumber

$F_{ij}$  : reduced force tensor, 2D

$F(t)$  : reduced force for 1D disturbance

$d_e(t)$  : current "equilibrium" thickness

$x_0$  : initial position of fluid cross section

$\delta_0(x_0)$  : initial thickness profile

$a(x,t)$  : disturbance amplitude (dimensionless,  $= \delta-1$ )

$a_0(x_0)$  : initial amplitude

$t_*$  : singular time for any cross section to reach infinite thickness

$\tau \equiv t-t_*$  : time relative to singular time

$L$  : length of layer, or wavelength of periodic disturbance

$L_0$  : initial length or wavelength

$\eta(x_0,t), f(\eta), \xi(\eta)$  : for similarity solutions describing plume

$x_*(t)$  : "initial" position of fluid section currently at plume position

$\alpha$  : arbitrary power for peak profile

$\varepsilon$  : small remainder

$\sigma$  : linearized growth rate

$\tau(\delta) \equiv t_{\star} - t$  : time until singularity for power-law fluid layer

$a(t), A(t), \xi(x,t), f(\xi), g(\xi)$  : for large-amplitude similarity solution



## 1. INTRODUCTION

This work describes the circumstances under which the motion of a buoyantly unstable horizontal film of viscous fluid is limited by normal viscous stresses, and gives an analysis showing how the growth of disturbances to the interface becomes greatly enhanced when the disturbance amplitude becomes large, leading to the formation of plumes in a finite time. A companion work will show that in certain cases this same dynamic balance controls the structure of the cold boundary layer in Bénard convection with strongly temperature-dependent viscosity. The behavior described here thus is of geophysical relevance to such flows as those in lava lakes, the thermal convection of planetary mantles, and possibly also in convection in the Earth's solid core. The Rayleigh-Taylor problem considered here is the simplest example of this dynamic balance.

The problem is illustrated in figure 1. Two layers of immiscible fluids are confined between shear-free boundaries, with the upper fluid layer being denser and much more viscous than the lower, and both fluids are so viscous that neither inertia nor surface tension is significant. A linearized analysis (appendix A) shows that the most unstable wavelength is long compared to the upper layer thickness. And scaling the problem shows that this fastest growth occurs in a broad range of wavelengths for which the lower fluid is effectively passive and hydrostatic. Thus we give a long-wave analysis, where the lower fluid is treated as inviscid, that exploits the fact that, for long waves, the disturbance amplitude can get very large (compared to the average layer thickness) while the slope of the interface remains small; this follows from mass conservation.

The results of this analysis show the nonlinear effects of large amplitude. In particular, it predicts that thickness maxima in the layer will reach infinite thickness in finite time, with the final catastrophic growth inversely proportional to the time remaining before the singular time. This conclusion is not unique to a Newtonian rheology; the corresponding analysis for a power-law fluid (appendix B) shows the same catastrophic inverse-time growth of large peaks.

The small-slope analysis predicts that at the singular time, a peak will locally have the shape  $\delta \propto |x|^{-2/3}$ , but that afterward, as the plume acts as a sink of fluid, the shape will change to  $\delta \propto |x|^{-1/2}$ .

Of course the small-slope approximation must fail before this, but we argue that the failure is only local; the slope remains small everywhere except in an asymptotically small neighborhood around each developing singularity. Furthermore, these small regions where the small-slope approximation breaks down have only an asymptotically small effect on the dynamics of the rest of the layer. Therefore the small-slope equations will continue to apply almost everywhere, even after the singular time, when peaks form downwelling plumes. (There is a family of similarity solutions, given in appendix C, that describe plume behavior.) Thus the same equations describe the disturbance from the initial linear growth through the rapid large-amplitude growth to the final draining of the layer by the plumes.

In the companion paper on the analogous thermally driven buoyant instability, there is a family of steady solutions (with plumes), and we use the small-slope equations to follow the development from initial conditions through to the final steady state.

## 2. PROBLEM STATEMENT

Two horizontal layers of distinct Newtonian incompressible fluids are bounded above and below by horizontal shear-free boundaries (see figure 1). The upper fluid (of density  $\rho_1$  and viscosity  $\mu_1$ ) is denser and much more viscous than the lower fluid (of density  $\rho_2 < \rho_1$  and viscosity  $\mu_2 \ll \mu_1$ ), and the upper layer is very thin ( $d_1 \ll d_2$ ). Both fluids are assumed to be so viscous that we can neglect both surface tension and inertia. The latter assumption requires

$$\Delta \rho g L^3 / \mu^2 \ll 1$$

where  $L$  is the largest length scale,  $\Delta \rho \equiv \rho_1 - \rho_2$ ,  $g$  is gravity,  $\rho$  is either density, and  $\mu$  is either kinematic viscosity; this is easily satisfied in mantle flow.

Initially both fluids are at rest in unstable equilibrium. Then at  $t = 0$  the interface is slightly disturbed; thereafter the interface position is given by  $\xi(x, y, t)$ . (Later we will assume that the disturbance varies only in the  $x$  direction; a one-dimensional disturbance allows some remarkable simplifications, and illustrates the physical behavior more clearly.)

A reduced pressure  $p$  is defined by:

$$P(x, y, z, t) = p(x, y, z, t) + \rho g(z - d_1) \quad (2.1)$$

where  $\rho$  is the local density ( $\rho_2$  or  $\rho_1$ ). Then the governing equations are:

$$\nabla p = \mu \nabla^2 \underline{u} \quad (2.2a)$$

$$\nabla \cdot \underline{u} = 0 \quad (2.2b)$$

and the boundary conditions are:

$$\text{at } z = 0 \text{ and at } z = (d_1 + d_2): w = u_z = 0 \quad (2.3a,b)$$

$$\text{at } z = \delta(x,y,t): [\underline{u}] = \underline{0}, \quad (2.3c)$$

$$[\hat{n}\underline{\sigma}] = \Delta\rho g(\delta - d_1)\hat{n}, \quad (2.3d)$$

$$\delta_t + u\delta_x + v\delta_y = w \quad (2.3e)$$

where  $[\ ]$  indicates the change in the enclosed quantity across the interface (downward),  $\underline{\sigma}$  is the reduced stress tensor, and the unit normal to the interface  $\hat{n}$  has components:

$$\hat{n} = ( -\delta_x, -\delta_y, 1 ) / \sqrt{(1 + \delta_x^2 + \delta_y^2)} \quad (2.4a)$$

Physically, the conditions (2.3a-d) are that the boundaries are impermeable and exert no shear, and across the interface both velocity and stress are continuous, while (2.3e) is the kinematic condition that the interface moves as a material surface.

These equations and boundary conditions, along with specification of the initial interface position  $\delta(x,y,0)$ , define the problem without approximation. To facilitate analysis, however, we limit attention to the development while the slope of the interface remains small, i.e.,  $\delta_x$  and  $\delta_y$  are both small. Then in the interface stress conditions we can approximate the unit normal, to lowest order, by:

$$\hat{n} = ( -\delta_x, -\delta_y, 1 ) \quad (2.4b)$$

and neglect any resulting terms quadratic in  $\delta_x$  and  $\delta_y$ . It should be noted that the resulting small-slope equations still retain the leading nonlinear terms due to slope and are still applied at  $z = \delta(x,y,t)$ , in contrast to the linearized conditions used for the small-amplitude analysis (appendix A).

The small-slope approximation applies trivially to small-amplitude disturbances. But more importantly, the small-slope approximation applies to long-wavelength disturbances even when the amplitude becomes large (until the

amplitude is comparable to the wavelength). Thus we can use the simplified equations to analyze the large-amplitude, nonlinear effects in long-wave instabilities, which we do in the next section.

### 3. LONG-WAVE ANALYSIS

The disturbance can grow in a variety of different ways, depending on the viscosity ratio, the depth ratio, and the dimensionless wavenumber:

$$\alpha \equiv \mu_2/\mu_1, \quad B \equiv d_2/d_1, \quad \epsilon \equiv kd_1 \quad (3.1)$$

(where the disturbance has a characteristic wavenumber  $k$ ). The linearized analysis in Appendix A gives the small-amplitude growth rates for the full range of all parameters. A scaling analysis (see Canright, 1987, App. B) shows that the same growth regimes apply even for large amplitudes, as long as the slope of the interface remains small.

Here we focus on the case where the lower fluid layer is much less viscous and deeper than the upper, so:

$$\alpha \ll 1, \quad B \gg 1 \quad (3.2)$$

Then there is a range of wavelengths, which includes the fastest growing wavelength, over which the growth rate is nearly constant (see fig 6):

$$\max(\alpha, \sqrt{\alpha/B}) \ll \epsilon \ll 1 \quad (3.3)$$

In this range, the growth is limited by normal stresses in the upper fluid, which moves nearly horizontally, while the lower fluid is passively moved by the interface. Outside this range, for waves short compared to  $d_1$ , the growth is reduced because only a fraction of layer 1 is mobilized, and for long enough waves the viscous resistance of fluid 2 slows the growth.

We examine the finite-amplitude growth of long-wave disturbances in this fastest-growth regime, exploiting the fact the slope of the interface remains small even for large amplitudes (until the disturbance grows to the order of

the initial wavelength). What follows is the leading-order asymptotic analysis; since the growth rate is constant to within  $O(\epsilon^4)$ , we cannot expect this analysis to predict the single wavelength giving maximum growth.

For wavelengths in this range, the interface motion is controlled by the dynamics of the upper fluid, while the lower fluid is effectively inviscid and hydrostatic; the error we make in neglecting the viscous resistance of the lower fluid is much smaller than  $O(\epsilon)$ . Hereafter we refer only to fluid layer 1 and drop the subscript 1 where clear. The motion is quasi-horizontal as both surfaces of the layer see no shear. It is driven by the horizontal variations of the buoyant pressure and resisted by the normal viscous stresses.

We now estimate the scales of the different terms, assuming for this purpose that the disturbance varies only in the  $x$  direction. Then there are two length scales,  $x \sim k^{-1}$ ,  $z \sim d_1$ , and  $\delta_x \sim \epsilon$ . From continuity (and the impermeable boundary),  $w/u \sim \epsilon$ . Consequently, comparing vertical and horizontal momentum equations shows that  $p_z/p_x \sim \epsilon$ , and the interface shear stress condition (2.3c) implies  $u_z \sim w_x$ , so  $u_z/u_x \sim \epsilon$ . The last scaling in turn implies that the variation of  $u$  across the layer is  $O(\epsilon^2)$  smaller than  $u$  (similarly for  $p$ ), though  $u_{zz} \sim u_{xx}$ .

When the initial disturbance to the interface varies in two dimensions, over a length scale long compared to the thickness of the upper layer but not so long that the resistance of the lower fluid becomes important, then the above scaling still applies. That is,  $u$ ,  $v$  and  $p$  are independent of  $z$ , and:

$$w = -z(u_x + v_y) \quad (3.4)$$

all within an error of  $O(\epsilon^2)$ . From the normal stress condition, to  $O(\epsilon^2)$ :

$$-p + \tau_{zz} = \Delta \rho g(\delta - d_1) \quad (3.5)$$

where  $\tau_{ij}$  is the deviatoric stress tensor.

Consider a force balance in the  $x$  direction on a small column of layer 1 (see figure 10). We reduce the force on all surfaces by the hydrostatic pressure gradient due to fluid 2; this does not affect the balance. Recalling (2.1) and from (3.5), the difference in total pressures is:

$$P_1 - P_2 = p + \Delta \rho g(z - d_1) = \tau_{zz} - \Delta \rho g(\delta - z) \quad (3.6)$$

Then the reduced force balance involves only the sides of the column, since the boundary is shear-free and the reduced force on the interface is zero, so:

$$\begin{aligned} \int_y^{y+\Delta y} [F_{xx}(x+\Delta x) - F_{xx}(x)] dy + \int_x^{x+\Delta x} [F_{xy}(y+\Delta y) - F_{xy}(y)] dx &= 0 \quad (3.7) \\ F_{xx} &\equiv \int_0^\delta [-(P_1 - P_2) + \tau_{xx}] dz \approx [\Delta \rho g \delta^2 / 2 + \delta(\tau_{xx} - \tau_{zz})] \\ F_{xy} &\equiv \int_0^\delta \tau_{xy} dz \approx [\delta \tau_{xy}] \end{aligned}$$

where  $F_{ij}$  is a 2-D tensor representing the reduced force in the layer: any vertical plane through the layer defines a horizontal normal direction, and the product of that normal and the tensor  $F_{ij}$  gives the reduced force vector acting on that plane. Dividing by  $\Delta x \Delta y$  and taking the limit as  $\Delta x, \Delta y \rightarrow 0$ :

$$\partial/\partial x(F_{xx}) + \partial/\partial y(F_{xy}) = 0 \quad (3.8)$$

Indeed, a force balance in the  $y$  direction shows:

$$\partial/\partial x_j(F_{ij}) = 0 \quad (3.9)$$

$$F_{ij} = \delta(-\bar{P} \delta_{ij} + \tau_{ij})$$

$$\bar{P} \equiv -\Delta \rho g \delta / 2 + \tau_{zz}$$

where  $\bar{P}$  is the average (reduced) pressure and  $\delta_{ij}$  is the Kronecker delta.

The kinematic interface condition becomes:

$$D\delta/Dt \equiv \delta_t + u\delta_x + v\delta_y = -\delta(u_x + v_y) \quad (3.10)$$

These two equations (3.9-10) govern the growth of long-wave disturbances.

Note that the above derivation is independent of the rheology of the fluid layer; any constitutive relation could be specified.

The analysis simplifies considerably for a one-dimensional disturbance; we develop only this case. In general, the reduced force  $F_{ij}$  is a two-dimensional tensor with zero divergence, reflecting the balance of buoyant and viscous forces in the layer. However, when the disturbance is one-dimensional, then only one component of  $F_{ij}$  is nonzero; we call this scalar  $F$ . Then (3.9-10) become:

$$\partial/\partial x \ F = 0 \quad (3.11)$$

$$D\delta/Dt \equiv \delta_t + u\delta_x = -\delta u_x \quad (3.12)$$

the former of which integrates directly to give:

$$4\delta u_x + (\Delta\rho g/\mu)\delta^2/2 = F(t) \quad (3.13)$$

This says that the force on any cross section of the layer, reduced by the hydrostatic pressure force due to the lower fluid, is the same everywhere in the layer, i.e.,  $F(t)$ . (This result is not surprising, in that the only outside force on the layer is just the external hydrostatic head.)  $F(t)$  depends on the conditions specified at the ends of the layer, e.g., if the layer had abrupt ends with no applied force, surrounded by fluid 2,  $F$  would be zero. Arbitrary end conditions can thus be incorporated via  $F(t)$ .

We will treat three cases where  $F$  is simple to evaluate. In the first case, the layer is of infinite extent, but the disturbance is localized, so that far away the layer remains in (unstable) equilibrium, and  $F$  is constant. This case has a simple analytic solution that illustrates clearly the nonlinear effects of finite amplitude. The second case is a periodic disturbance (or equivalently, a layer with shear-free end walls). Here, the requirement that  $u = 0$  at both ends of a period determines  $F(t)$  as an integral



property of the shape of the layer. In the last (and simplest) case the layer is of finite extent so  $F = 0$ ; this solution also applies approximately when  $\delta$  is large and  $F$  can be neglected.

In dimensionless form, the governing equations (3.12-13) become:

$$D\tilde{\delta}/D\tilde{t} \equiv \partial\tilde{\delta}/\partial\tilde{t} + \tilde{u}\partial\tilde{\delta}/\partial\tilde{x} = -\tilde{\delta}\partial\tilde{u}/\partial\tilde{x} \quad (3.14)$$

$$\tilde{\delta}\partial\tilde{u}/\partial\tilde{x} + \tilde{\delta}^2 = \tilde{F}(\tilde{t}) \equiv \tilde{d}_e^2(\tilde{t}) \quad (3.15)$$

which can be combined to eliminate  $u$  by adopting a Lagrangian formulation, where the fluid "particle" in this case is a material cross section of the layer, to give:

$$D\tilde{\delta}/D\tilde{t} = \tilde{\delta}^2 - \tilde{d}_e^2(\tilde{t}) \quad (3.16)$$

Here  $D/Dt \equiv \partial/\partial t + u\partial/\partial x$  is the time derivative following a fluid cross section,  $\tilde{\delta} \equiv \delta/d_1$ ,  $\tilde{t} \equiv \sigma t$ ,  $\sigma \equiv \Delta\rho g d_1/(8\mu)$  is half the small-amplitude growth rate,  $\tilde{x} \equiv kx$ ,  $\tilde{u} \equiv ku/\sigma$ ,  $k$  is the wavenumber, and  $\tilde{d}_e(\tilde{t}) \equiv [F(t)/(\Delta\rho g d_1^2/2)]^{1/2}$  is the current (nondimensional) equilibrium thickness, i.e., that thickness with no tendency to grow or shrink, so  $\tilde{d}_e(0) = 1$ . Equation (3.16) is a Ricatti equation, and can be integrated analytically for several different forms of  $\tilde{d}_e(\tilde{t})$ , or numerically for arbitrary  $\tilde{d}_e(\tilde{t})$ .

This result shows that the vertical motion of the interface depends only on the local layer thickness and the current equilibrium thickness (which may depend on the overall shape of the whole layer). Thus any fluid cross section does not care what its immediate neighbors are doing, and the growth is insensitive to wavelength, as expected. Of course, the horizontal motion of any cross section depends on the shape of the whole layer.

## 4. SOLUTIONS

### 4.1. LOCALIZED DISTURBANCE

The most illustrative case is an infinite layer with a disturbance of finite extent. Then the force on the ends of the disturbed region remains constant:  $\tilde{d}_e = 1$ . This has a simple solution (drop tildes):

$$\delta(x_0, t) = \frac{(1 + A(x_0)e^{2t})}{(1 - A(x_0)e^{2t})}, \quad A(x_0) \equiv \frac{(\delta_0(x_0) - 1)}{(\delta_0(x_0) + 1)} \quad (4.1)$$

where  $\delta_0(x_0) \equiv \delta(x_0, t=0)$  and  $x_0$  identifies a particular fluid cross section by its initial position. This becomes singular in finite time: when  $t = t_* \equiv \ln|1/A|$  the thickness  $\delta$  goes to  $\infty$  or 0, depending on whether  $\delta_0$  was greater or less than 1. (When the minimum thickness in the layer first reaches zero, then  $d_e$  becomes zero, and the above solution becomes invalid for the entire layer.)

When the initial perturbation amplitude  $a_0(x_0) \equiv \delta_0(x_0) - 1$  is small, the solution reduces to:

$$\delta \approx \frac{1 + a_0 e^{2t}/2}{1 - a_0 e^{2t}/2} + O(a_0^2 e^{2t}) \quad (4.2a)$$

and while the amplitude  $a(x_0, t) \equiv \delta(x_0, t) - 1$  remains small:

$$a \approx a_0 e^{2t} (1 + a_0 (e^{2t} - 1)/2) \quad (4.2b)$$

Initially this gives the exponential growth of the linearized solution, and as nonlinearities become important the perturbation growth accelerates for peaks ( $a > 0$ ) and retards for troughs ( $a < 0$ ). As a result of this and volume conservation, the peaks get narrower and sharper while the troughs broaden and flatten. We can roughly estimate the duration of the linear behavior by when this small-amplitude solution gives  $a \sim 1$ :  $\Delta t \sim \ln|1/a_0|$ .

As the amplitude gets large, the growth becomes algebraic in the time remaining before the thickness becomes singular ( $\infty$  or 0):

$$\delta_0 > 1: \delta \approx 1/(t_\star - t) \quad (4.3a)$$

$$\delta_0 < 1: \delta \approx t_\star - t \quad (4.3b)$$

which shows that the rapid nonlinear growth occurs over a time  $\Delta t \sim 1$ , or, dimensionally,  $8\mu/\Delta\rho g d_1$ .

The catastrophic growth shown by the inverse relation (4.3a) between peak thickness and remaining time is strikingly different from the exponential growth of small amplitudes. For large peaks the relevant time scale is the time remaining before the singularity, which is inversely proportional to the current dimensional peak thickness  $\delta_{\max}$ :  $t \sim \mu/\Delta\rho g \delta_{\max}$ . This shows that large-amplitude effects drastically enhance the growth of peaks.

To see the shape of the layer requires Eulerian coordinates. As  $x$  is the integral of the strain  $dx/dx_0$ , and because volume in the layer (and in each fluid cross section) is conserved,  $dx/dx_0 = \delta_0/\delta$ :

$$x(x_0, t) = \int_0^{x_0} \delta_0(x_0)/\delta(x_0, t) dx_0 \quad (4.4)$$

where the  $x$  origin is chosen at some stationary fluid cross section.

We find that, at least initially, the overall strain increases, i.e., the perturbed section stretches out in the  $x$  direction, for any initial perturbation with a zero mean. To see this, we take the time derivative of the position  $L$  of the end of the disturbed region:

$$DL/Dt = \int_0^{L_0} \delta_0(1-\delta^2)/\delta^2 dx_0 \quad (4.5a)$$

Then at  $t = 0$ , in terms of the amplitude  $a(x, t)$ :

$$DL/Dt = \int_0^L (-2a + a^2/\delta) dx = \int_0^L a^2/\delta dx > 0 \quad (4.5b)$$

since  $\int a dx = 0$ . That the disturbed region stretches out in the  $x$  direction

is surprising, but is entirely consistent with the assumption that the force on the ends remains constant.

For example, if the initial perturbation is sinusoidal we get:

$$\delta_0 = 1 - b \cos x_0 \quad (4.6a)$$

$$\delta(x_0, t) = \frac{2 - b(1+e^{2t}) \cos x_0}{2 - b(1-e^{2t}) \cos x_0} \quad (4.6b)$$

$$x(x_0, t) = bC \sin x_0 + (D-C)x_0 + \frac{2CD}{\sqrt{(E^2-b^2)}} \arctan \frac{\sqrt{(E^2-b^2)} \tan(x_0/2)}{E-b} \quad (4.6c)$$

$$C \equiv (e^{2t}-1)/(e^{2t}+1), D \equiv 4e^{2t}/(e^{2t}+1)^2, E \equiv 2/(e^{2t}+1) \quad (4.6def)$$

and the overall strain is  $D-C + CD/\sqrt{(E^2-b^2)}$ , which increases monotonically with time. This solution is graphed as  $\delta(x)$  for various times in figure 2.

When the initial amplitude  $b$  is small, the solution simplifies:

$$\delta \approx \frac{1 + A \cos x_0}{1 - A \cos x_0}, \quad A(t) \equiv b e^{2t}/2 \quad (4.6g)$$

$$x \approx \frac{4}{\sqrt{(1-A^2)}} \tan^{-1} \left[ \frac{\sqrt{(1-A)}}{\sqrt{(1+A)}} \tan(x_0/2) \right] - x_0 \quad (4.6h)$$

#### 4.2. CONSTANT WAVELENGTH DISTURBANCE

For the second case, we consider the more physically reasonable situation of a layer of finite extent bounded by fixed (shear-free) end walls (or the equivalent situation of a periodic disturbance of infinite extent). Then the end forces must vary with time to give  $u = 0$  at both ends. Integrating (3.9) in  $x$  shows that fixed ends require:

$$d_e^2(t) = \left( \int_0^L \delta \, dx \right) / \left( \int_0^L 1/\delta \, dx \right) \quad (4.7)$$

where  $L$  is the entire length of the layer (or one wavelength), so the numerator is just the total volume of fluid in the layer, a constant. Thus

the thinnest parts of the layer have the greatest effect on  $d_e(t)$ . We find that, as a result of (4.7),  $d_e(t)$  decreases in general, although the effect is small for small amplitude. As the disturbance grows and the troughs deepen and broaden while the peaks become narrower,  $d_e$  can only decrease with time.

Combining (4.7) and (3.10) (using  $dx = (\delta_0/\delta)dx_0$ ) gives a single partial integro-differential equation that can be solved numerically for  $\delta(x_0, t)$  given an arbitrary initial profile  $\delta_0(x_0)$ :

$$D\delta/Dt = \delta^2 - \left( \int_0^L \delta_0 dx_0 \right) / \left( \int_0^L \delta_0/\delta^2 dx_0 \right) \quad (4.8)$$

For large amplitude, the main effect of fixed wavelength is to slow the growth of troughs; in fact,  $\delta$  is prevented from reaching zero. In contrast, peak growth is only slightly accelerated. When peaks become large, then  $d_e$  becomes negligible in comparison, as in the constant  $d_e$  case, but sooner here since  $d_e$  decreases. Thus large peaks show the same catastrophic growth to infinite thickness, given by (4.3a). Therefore the growth of large peaks, where  $d_e$  is unimportant, is insensitive to (reasonable) end conditions, and our previous conclusion, that the growth of peaks is dramatically enhanced by large-amplitude effects, applies in general.

Qualitatively this case is very similar to the previous, as shown by the profiles in figure 3, except that the wavelength remains constant. Figure 4 compares the growth of the peak for fixed wavelength with that for constant end forces, each for an initial sinusoidal disturbance.

#### 4.3. LARGE-AMPLITUDE BEHAVIOR

Where  $\delta \gg d_e$ , we can approximate (3.16) by

$$D\delta/Dt = \delta^2 \quad (4.9)$$

(This would apply without approximation if the layer were of finite extent, surrounded by fluid 2.) This integrates to:

$$\delta(x_0, t) = 1/(1/\delta_0(x_0) - t) \quad (4.10)$$

where again  $\delta_0(x_0)$  is the initial profile. Thus each cross section reaches infinite thickness at time  $t_* = 1/\delta_0$ ; this is the same growth as (4.3a).

For this case, (3.15) simplifies to:

$$\delta + u_x = 0 \quad (4.11)$$

so

$$u(x, t) = - \int_0^x \delta(s, t) ds \quad (4.12)$$

where the origin is assumed to be stationary. As long as  $\delta$  remains finite everywhere, we can use  $\delta dx = \delta_0 dx_0$ , so:

$$u(x_0) = - \int_0^{x_0} \delta_0(s) ds \quad (4.13)$$

which shows that each cross section moves at a uniform speed until the maximum thickness reaches the singular time. These results (4.10, 4.12) apply locally around any large peak where  $d_e$  is negligible.

## 5. PLUME FORMATION

Here we examine what happens to a thickness maximum as it approaches the singular time ( $t_*$ ). We will show how the peak becomes a plume, where the dense, viscous fluid drains down. We argue that the small-slope equations still describe the behavior of the fluid, except in an asymptotically small neighborhood of the plume. This is possible because that neighborhood has only an asymptotically small effect on the stress in the layer. Thus we can describe the shape of the layer around the plume, and the small-slope equations can be used all the way from initial conditions through the final draining of the layer.

As the maximum grows, clearly the small-slope assumption must break down locally before the peak reaches infinite thickness; at what thickness it breaks down depends on the initial wavelength of the disturbance. Since the

initial disturbance wavelength is asymptotically long, or equivalently, the layer is initially asymptotically thin ( $\epsilon \equiv kd_1 \ll 1$ ), then when the peak reaches infinite thickness, that portion of the layer around the peak where the physical slope of the interface is  $O(1)$  or greater will be asymptotically narrow compared to the whole wavelength. This follows from mass conservation, and from the shape near the peak approaching (as we will show) an integrable negative power of  $x$  (where for convenience we have chosen  $x = 0$  at the peak). This point is illustrated in figure 5. So the small-slope approximation continues to apply almost everywhere in the layer; what is needed is a description of the effect of the peak or plume on the rest of the layer

In a companion paper, we give a large-slope analysis appropriate to the region around a peak where the small-slope approximation no longer applies. There the flow is extensional, nearly vertical, driven by buoyancy and limited by normal viscous stresses. We find that large-slope effects do not slow down the growth, they only affect the detailed shape of the peak. Specifically, we find that the catastrophic behavior described by (4.3a) still applies (except for a numerical coefficient close to 1). Physically, there is nothing to prevent the fluid from flowing down. In this way, the peak extends to become a plume, where the viscous fluid continues to drain down. Of course, at some point the fluid will reach the lower boundary or the extending peak will become so long that the viscous resistance of fluid 2 becomes important. In the former case, only the details of the plume shape are changed, but in the latter, the driven flow in fluid 2 could affect the dynamics of the upper layer.

To the rest of the layer the plume appears as an isolated singularity, a sink of fluid. The horizontal force balance must still apply even to the

plume, and so the reduced force in the layer  $F(t)$  is continuous across the plume. Recall that  $F(t)$  is an integral property of the whole layer; for a fixed-wavelength disturbance the dimensionless form is given by (4.7). Because the region where the small-slope approximation fails is integrable (as it must be, since no new mass is created) and asymptotically thin, its effect on  $F(t)$  is negligible. Equation (4.7) shows that where  $\delta$  is largest has the smallest effect on  $F$ . (Even after fluid starts draining out of the layer, the numerator in (4.7) still just gives the volume of the layer, regardless of its shape.)

As an example, consider what happens near the maximum when the initial disturbance is a small-amplitude sinusoid. (For simplicity, we assume the constant-force end conditions, but as  $F$  has little effect on a large peak the results apply to more general end conditions.) The previous solution (4.6g,h) shows that the peak becomes singular as  $A \equiv be^{2t}/2$  approaches unity. Then in (4.6h) the argument of the inverse tangent approaches zero (for  $x_0$  away from  $\pi$ ), so near the singular time (4.6h) becomes:

$$x \approx 2 \tan(x_0/2) - x_0 \quad (5.1a)$$

for  $(1-A) \ll 1$ , and  $(1-A)^{1/3} \ll (\pi - x_0)$ . Then near the peak ( $x_0 \ll 1$ ):

$$x \approx x_0^3/12 \quad (5.1b)$$

Setting  $A = 1$  in (4.6g) gives the thickness profile at the singular time:

$$\delta \approx \cot^2(x_0/2) \quad (5.2a)$$

and near the peak:

$$\delta \approx (x_0/2)^{-2} \approx (3/2 x)^{-2/3} \quad (5.2b)$$

This shows that at the singular time the peak becomes proportional to an integrable negative power of  $x$ .



In fact, any smooth initial peak results in the same power of  $x$ . For  $x_0 \ll 1$ , the smooth (symmetric) initial peak is asymptotically:

$$\delta_0 \approx 1 + b(1 - cx_0^2/2) + O(bx_0^4) \quad (5.3)$$

where  $b$  is the (small) initial amplitude and  $c$  is some positive constant.

Then from (4.2a):

$$\delta \approx \frac{1 + A(1 - cx_0^2/2)}{1 - A(1 - cx_0^2/2)} \quad (5.4a)$$

where again  $A(t) \equiv be^{2t}/2$ . Near the singular time,  $A \rightarrow 1$  and:

$$\delta \rightarrow \frac{2}{(1-A) + cx_0^2/2} \quad (5.4b)$$

From continuity,  $dx/dx_0 = \delta_0/\delta \approx 1/\delta$  (for small initial amplitude), so for  $x_0 \ll 1$  and as  $A \rightarrow 1$ :

$$x \rightarrow (1-A)x_0/2 + cx_0^3/12 \quad (5.5)$$

At the singular time,  $A = 1$ , and near the singularity:

$$\delta \approx 4/(cx_0^2) \approx c^{-1/3} (3x/2)^{-2/3} \quad (5.6)$$

For the sinusoidal disturbance,  $c = 1$  and (5.6) reduces to (5.2b).

As the singular time is approached, the peak can be described by a similarity solution. Defining  $\eta(x_0, t)$  by:

$$(1-A(t))\eta^2 \equiv cx_0^2/2 \quad (5.7a)$$

reduces (5.4b, 5.5) to:

$$f(\eta) \equiv (1-A)\delta/2 = 1/(1+\eta^2) \quad (5.7b)$$

$$\xi(\eta) \equiv 3\sqrt{2c}(1-A)^{-3/2} x = \eta^3 + 3\eta \quad (5.7c)$$

This is a particular case of the general similarity solution for large  $\delta$  given in appendix D. The comparison is clarified by noting that:

$$A \equiv e^{2\tau}, \quad \tau \equiv t - t_* \quad (5.8a)$$

so that as  $A \rightarrow 1$ ,  $\tau \rightarrow 0$ , then to leading order in  $\tau$ :

$$(1-A) + 2\tau \quad (5.8b)$$

The general similarity solution shows that a peak of the more general form  $\delta_0 \approx 1 + b(1 - c|x_0|^n)$ , where  $n > 0$ , gives a singularity of the form  $\delta(x, t_*) \propto |x|^{-m}$ , where  $m = n/(n+1)$ . In other words, any (reasonable) initial peak becomes, at  $t_*$ , a singularity proportional to an integrable negative power of  $x$ .

After the peak becomes singular (i.e., a plume) the shape of the layer around the plume can be calculated using the large-amplitude forms of the equations given in section 4.3. For simplicity, we assume  $\delta$  is symmetric in  $x$ , decreasing monotonically away from the origin, and we only consider  $x > 0$ . Also, we choose the time origin such that the "initial" amplitude  $\delta_0 \gg d_e$  in the region of interest. Then the large-amplitude equations apply:

$$\delta(x_0, t) = 1/(1/\delta_0(x_0) - t) \quad (4.10)$$

$$u(x, t) = - \int_0^x \delta(s, t) ds \quad (4.12)$$

The peak becomes infinite at  $t_* = 1/\delta_0(0)$ . Thereafter, the layer must move in such a way that each fluid cross section reaches the origin at the same time that it reaches infinite thickness. In other words, if for  $t > t_*$  we designate the fluid element  $x_0$  at the singularity by  $x_0 = x_*(t)$ , so  $x_*(t_*) = 0$ , then  $\delta_0(x_*(t)) = 1/t$ , and since  $\delta_0$  is an invertible function by the assumptions above, this uniquely defines  $x_*$ , and thus also determines the strength ( $\delta_0(x_*)dx_*/dt$ ) of the sink at the singularity, as a function of time. With these large-amplitude equations we can determine the shape around the singularity for all time.

Now we consider the fate of the inverse power of  $x$  singularity that forms at  $t_*$ :

$$\text{at } \tau = 0: \delta_0(x_0) = \delta(x=x_0, t=t_*) = b x_0^{-\alpha}, \quad 0 < \alpha < 1 \quad (5.9a)$$

where we have chosen the reference time at  $t_*$ , when  $\tau \equiv t - t_* = 0$ , and  $b$  is some positive amplitude. Then the fluid cross section  $x_0$  at the origin is specified by  $x_0 = x_*(\tau)$ , where:

$$x_*(\tau) = (b\tau)^{1/\alpha} \quad (5.9b)$$

Using (4.10) shows that:

$$\delta(x_0, \tau) = b/(x_0^\alpha - x_*^\alpha) \quad (5.9c)$$

so:

$$\begin{aligned} x(x_0, \tau) &= \int_{x_*}^{x_0} \delta_0(s)/\delta(s, \tau) ds \\ &= (x_0 - x_*) - (x_*^\alpha/(1-\alpha))(x_0^{1-\alpha} - x_*^{1-\alpha}) \end{aligned} \quad (5.9d)$$

Far away from the plume ( $x_0 \gg x_*$ ), the profile is still the starting profile from  $\tau = 0$  ( $x \approx x_0$ ,  $\delta \approx bx^{-\alpha}$ ). However, very close to the plume:

$$x_0 = x_*(1+\epsilon), \quad \epsilon \ll 1 \quad (5.9e)$$

$$x \approx \alpha x_* \epsilon^2/2 \quad (5.9f)$$

$$\delta/b \approx 1/(\alpha \epsilon x_*^\alpha) \approx (b\tau)^{1/(\alpha-1)}/\sqrt{2\alpha x} \quad (5.9g)$$

This shows that asymptotically near the plume, the singularity goes like  $1/\sqrt{x}$ , with a scale that varies in time. This asymptotic  $x$  dependence is actually independent of the starting conditions (as shown by Canright, 1987, App. C). From (5.9g) it is clear that whether  $\delta$  near the plume grows or shrinks is determined by whether  $\alpha < 1/2$  or  $\alpha > 1/2$ , respectively. The special case  $\alpha = 1/2$  gives a steady solution. For  $\alpha > 1/2$ , the fluid drains away down the plume faster than it comes in from the sides, and the square-root singularity diminishes with time as it spreads out, to match onto the nearly undisturbed profile  $x^{-\alpha}$ . This would be the eventual fate of an initially ( $t = 0$ ) smooth maximum, which gives  $\alpha = 2/3$ . Conversely, if  $\alpha < 1/2$ , the square-root singularity grows as it spreads, fed from the sides faster than it can drain fluid away. (To get  $\alpha < 1/2$  would require a cusp-

like initial maximum, which may not be physically realistic.) This solution (5.9a-g) is again a particular case of the general large-amplitude similarity solution of appendix D. To see this, define  $n(x_0, \tau)$ :

$$n(x_0, \tau) \equiv x_0/x_*(\tau), \quad n \geq 1 \quad (5.10a)$$

$$f(\eta) \equiv \tau \delta = 1/(\eta^\alpha - 1) \quad (5.10b)$$

$$\xi(\eta) \equiv x/x_*(\tau) = \eta - (\eta^{1-\alpha} - \alpha)/(1-\alpha) \quad (5.10c)$$

With the above description of how a plume first forms and how it behaves afterward, the small-slope equations can be used to follow the development of the instability from initial conditions through rapid large-amplitude growth all the way to the draining away of the fluid down the plumes. The results will be inaccurate wherever the physical slope of the interface is not small, but such regions comprise only a small fraction of the domain. The only assumption is that a plume does not exert any net horizontal force on the surrounding layer. This assumption may break down if a plume's length becomes so much greater than the initial wavelength that the flow it drives in fluid 2 becomes dynamically significant.

## 6. CONCLUSIONS

The central concern of this work is the nonlinear interactions between buoyant forces and normal viscous stresses that occur in a buoyantly unstable viscous layer under a shear-free horizontal boundary and over a much less viscous fluid, for long-wave disturbances in the range where the lower fluid is dynamically unimportant. After the initially uniform thickness of the layer has been perturbed slightly, the early growth of the (small) perturbation is exponential; the perturbation keeps its shape while it grows. But when the nonlinearities become important, the thicker parts of the layer thicken more rapidly while the thinner parts thin more slowly, giving in

general sharp peaks with broad, flat troughs in between. The accelerating growth of peaks leads to infinite thickness at some time  $t_*$  (which depends on initial conditions), and the final catastrophic growth of the peak thickness  $\delta$  is algebraic:  $\delta \approx \mu / \Delta \rho g (t_* - t)$ . (In fact, this same sort of inverse-time catastrophic growth is also predicted for a power-law fluid, though the coefficient is different.) This shows how large-amplitude growth is fundamentally different from small-amplitude growth; large-amplitude effects dramatically enhance the growth of peaks.

These are the results of a small-slope analysis; of course, where the peaks become very large the small-slope approximation breaks down and there the flow becomes fully two-dimensional. But as a companion work that employs a large-slope analysis will show, the growth of the disturbance at large slopes is essentially the same as that predicted here, with catastrophic inverse-time peak growth; although the details of the peak shape do change, this only changes the prediction by a numerical factor of order 1.

Furthermore, the small-slope equations will continue to apply to the layer even after the formation of downwelling plumes, except in an asymptotically narrow neighborhood around each plume. This is possible because the plumes do not change the horizontal force balance (unless the flow they drive in the lower fluid becomes dynamically significant). Applying the equations up to the singular time shows that the first singularity should have the local shape  $\delta \propto |x|^{-2/3}$ , but that afterwards, as the plume drains the layer, the singularity changes shape to  $\delta \propto |x|^{-1/2}$ . This behavior is clarified by a family of similarity solutions, appropriate where  $\delta$  is large.

Thus the small-slope analysis can be extended to describe the development

of the layer for all time, except in those narrow regions where the physical slope of the interface becomes large.

## APPENDICES

### A. LINEARIZED SOLUTION

Here we calculate initial growth rates for the general problem with arbitrary wavelength, depths, and viscosities. Initially the perturbations are small, so the problem can be linearized by applying the interface conditions at  $z = d_1$  and assuming the slope remains small, but of course including the buoyant pressure term due to the perturbations. (This is an extension of the analysis given by Whitehead and Luther, 1975, to include the effects of finite depth in fluid 2.) Thus the interface conditions (2.3c-f) become:

$$\text{at } z = d_1: [\underline{u}] = [\mu(u_z + w_x)] = 0 \quad (\text{A.1a})$$

$$[-p + 2\mu w_z] = \Delta\rho g(\delta - d_1) \quad (\text{A.1b})$$

$$\delta_t = w \quad (\text{A.1c})$$

where again  $[\ ]$  indicates the jump in value from fluid 1 to fluid 2. Then the equations are separable, and a simple analytical solution is possible. The perturbation is assumed to be sinusoidal, but as the problem is linear, any (small) initial condition can be constructed by superposition.

The solution is given below, where the subscripts 2 and 1 refer to the two fluids,  $k$  is the wave number,  $a(t)$  is the dimensionless amplitude,  $Z \equiv z - (d_1 + d_2)$  is the coordinate in fluid 2,  $\alpha \equiv \mu_2/\mu_1$  is the viscosity ratio, and in the coefficients  $A, B, E, F$ , and their common denominator  $D$  these abbreviations are used:  $\tilde{k} \equiv 2kd_1$ ,  $\tilde{K} \equiv 2kd_2$ ,  $c \equiv \cosh(\tilde{k})$ ,  $C \equiv \cosh(\tilde{K})$ ,  $s \equiv \sinh(\tilde{k})$ ,  $S \equiv \sinh(\tilde{K})$ .

$$\delta = d_1 [1 + a(t) \cos(kx)] \quad (\text{A.2a-j})$$

$$\psi_1 = (\Delta \rho g d_1 / \mu_1 k^2) a(t) / 2 \sin(kx) [A \sinh(kz) + B kz \cosh(kz)]$$

$$\psi_2 = (\Delta \rho g d_1 / \mu_1 k^2) a(t) / 2 \sin(kx) [E \sinh(kZ) + F kZ \cosh(kZ)]$$

$$p_1 = (\Delta \rho g d_1) \{ -a(t) B \cos(kx) \cosh(kz) \}$$

$$p_2 = (\Delta \rho g d_1) \{ -a(t) \alpha F \cos(kx) \cosh(kZ) \}$$

$$A \equiv (-1/D) \{ [2(S-\tilde{K}) + \alpha \tilde{k}(C-1)] \sinh(kd_1) +$$

$$[\tilde{k}(S-\tilde{K}) + \alpha(\tilde{k}\tilde{K} + 2(C-1))] \cosh(kd_1) \}$$

$$B \equiv (2/D) \{ (S-\tilde{K} + \alpha \tilde{K}) \sinh(kd_1) + \alpha(C-1) \cosh(kd_1) \}$$

$$E \equiv (1/D) \{ [2\alpha(s-\tilde{k}) + \tilde{K}(c-1)] \sinh(kd_2) +$$

$$[\alpha \tilde{K}(s-\tilde{k}) + \tilde{K}\tilde{k} + 2(c-1)] \cosh(kd_2) \}$$

$$F \equiv (-2/D) \{ [\alpha(s-\tilde{k}) + \tilde{k}] \sinh(kd_2) + (c-1) \cosh(kd_2) \}$$

$$D \equiv (S-\tilde{K})(s+\tilde{k}) + 2\alpha(Cc-1+\tilde{K}\tilde{k}) + \alpha^2(S+\tilde{K})(s-\tilde{k})$$

Then from  $\delta_t = w(z=d_1)$  we get the growth rate:

$$a(t) = a(0) e^{\sigma t} \quad (\text{A.3a})$$

$$\sigma = (\Delta \rho g d_1 / \mu_1) \tilde{\sigma} \quad (\text{A.3b})$$

$$\tilde{\sigma} = \frac{1}{\tilde{k}} \frac{(S-\tilde{K})(c-1) + \alpha(s-\tilde{k})(C-1)}{(S-\tilde{K})(s+\tilde{k}) + 2\alpha(Cc-1+\tilde{K}\tilde{k}) + \alpha^2(S+\tilde{K})(s-\tilde{k})} \quad (\text{A.3c})$$

The symmetry of the problem is apparent in the solution. Had we chosen fluid 2 as the reference rather than fluid 1, the solution would have the same form. Thus we can, without loss of generality, assume that fluid 2 is the deeper layer:  $\tilde{K} > \tilde{k}$ .

This solution is governed by three independent dimensionless parameters: the non-dimensional wavenumbers, or depths,  $\tilde{k}$  and  $\tilde{K}$  (or equivalently  $\tilde{k}$  and the depth ratio  $\beta \equiv d_2/d_1$ ), and the viscosity ratio  $\alpha \equiv \mu_2/\mu_1$ . It should be noted that  $\tilde{\sigma}$  is a monotonically decreasing function of  $\alpha$ , i.e., if we increase  $\mu_2$

while  $\nu_1$  stays constant the growth rate can only decrease. Also note that if  $\beta \rightarrow \infty$  then (A.3c) reduces to:

$$\tilde{\sigma} = \frac{1}{\tilde{k}} \frac{(c-1) + \alpha(s-\tilde{k})}{(s+\tilde{k}) + 2\alpha c + \alpha^2(s-\tilde{k})} \quad (\text{A.3d})$$

which is just the result of Whitehead and Luther (1975). Figure 6a shows the effects of viscosity ratio on  $\tilde{\sigma}(\tilde{k})$  for  $\beta = \infty$ ; figure 6b shows the effects of finite depth for  $\alpha \ll 1$ .

When  $\beta \gg 1$  there are well defined regimes of growth where different force balances are dominant. These are shown schematically, with the corresponding growth rates, in figure 7. As we discuss the various growth mechanisms below, it should be kept in mind that the same mechanisms continue to apply as long as the slope of the interface remains small, which for long waves includes large-amplitude growth. (This point is supported by the scaling argument in Canright, 1987, App. B.)

For sufficiently short waves ( $\tilde{k} \gg \min(1, \max(\beta^{-1}, \alpha^{-1/3}))$ ) the disturbance sees neither boundary and  $\tilde{\sigma} \rightarrow [\tilde{k}(1+\alpha)]^{-1}$ , so if one viscosity is much larger, that one limits the growth. The dominant mechanism here is that the vertical motion of the interface is resisted by normal viscous stresses in the more viscous fluid, and the growth rate diminishes with decreasing wavelength.

At the other extreme, for sufficiently long waves ( $\tilde{k} \ll \min(\beta^{-1}, \sqrt{(\beta/\alpha)}, \sqrt{(\alpha\beta)})$ ) the boundaries confine the flow to be mainly horizontal, limited by shear stresses at the interface. Then  $\tilde{\sigma} \rightarrow \tilde{k}^2(1+\beta/\alpha)/12$ , and the controlling viscosity depends on if  $\alpha > \beta$  or not.

Between these extremes, the waves are long compared to layer 1 so the motion of the interface is primarily horizontal, and there are four different regimes. In one ( $\alpha^{-1} \ll \tilde{k} \ll \alpha^{-1/3}$ ,  $1 \ll \alpha \ll \beta^3$ ), fluid 2 is relatively



immobile and the growth is limited by the shear across layer 1, giving the same growth rate as the previous case, i.e.,  $\tilde{k}^2/12$ . (This possibility was apparently overlooked by Whitehead and Luther.) In another ( $\beta^{-1} \ll \tilde{k} \ll \min(\alpha, \alpha^{-1})$ ), the slight resistance of fluid 2 (the rate-controlling viscosity is  $\mu_2$ ) gives a small shear gradient across layer 1, which over the long wavelength is sufficient to balance the buoyancy, giving  $\tilde{\sigma} \rightarrow \tilde{k}/4\alpha$ .

In the other two regimes, the less viscous fluid is effectively passive, and the primarily horizontal motion of the more viscous layer is limited by normal viscous stresses. The resulting growth rate is nearly independent of wavelength, and includes the maximum growth rate possible for a given viscosity contrast  $\alpha$  where this behavior occurs. (For other  $\alpha$ , i.e.,  $1 \ll \alpha \ll \beta^3$ , we expect the fastest growth at the crossover between short- and long-wave behavior, at  $\tilde{k}_{\max} \approx 2.9/\alpha^{1/3}$ ,  $\tilde{\sigma}_{\max} \approx 0.23/\alpha^{2/3}$ .) When fluid 2 is much more viscous ( $\alpha \gg \beta^3$ ), this regime ( $\sqrt{\beta/\alpha} \ll \tilde{k} \ll \beta^{-1}$ ) gives  $\tilde{\sigma} \rightarrow \beta/4\alpha$ , while for fluid 1 more viscous ( $\alpha \ll 1$ ) this regime ( $\max(\alpha, \sqrt{\alpha\beta}) \ll \tilde{k} \ll 1$ ) gives  $\tilde{\sigma} \rightarrow 1/4$ .

In the last case, consideration of higher-order effects shows that, for  $\beta^{-5} \ll \alpha \ll 1$ ,  $\tilde{\sigma} \approx (1/4)(1 - (\alpha/\tilde{k} + \tilde{k}^4/720))$ . This broad maximum peaks at  $\tilde{k}_{\max} \approx (130\alpha)^{1/5} = 2.8 \alpha^{1/5}$  and  $\tilde{\sigma}_{\max} \approx (1/4)(1 - 0.44 \alpha^{4/5})$ . As an indication of the flatness of this peak, for the range  $\alpha^{4/5} < \tilde{k} < 5.2 \alpha^{1/20}$ ,  $\tilde{\sigma} \approx (1/4)(1 - \alpha^{1/5})$ . When  $\alpha \ll \beta^{-5}$ , the finite depth modifies the maximum growth rate giving  $\tilde{\sigma} \approx (1/4)(1 - (3\alpha/\beta\tilde{k}^2 + \tilde{k}^4/720))$  with a broad peak at  $\tilde{k}_{\max} \approx 3.2(\alpha/\beta)^{1/6}$  and  $\tilde{\sigma}_{\max} \approx (1/4)(1 - 0.44(\alpha/\beta)^{2/3})$ .

The present work is only concerned with the case of a thin, viscous layer over a less viscous, deep layer, so  $\alpha \ll 1$  and  $\beta \gg 1$ . We further restrict

our consideration to the mechanism giving the fastest growth, i.e., the last regime considered above, where  $\tilde{\sigma} \approx 1/4$ . The lowest-order finite-amplitude analysis (section 3) therefore predicts that the growth is independent of wavelength.

#### B. POWER-LAW FLUID

The long-wave quasi-one-dimensional analysis of section 3 is not limited to Newtonian rheology; any constitutive relation can be accommodated. The important point is that both surfaces of the layer are shear-free (in the wavelength range where the lower fluid is passive), so throughout the layer shear stresses are  $O(\epsilon)$  smaller than normal stresses, and the latter are independent of  $z$  to  $O(\epsilon^2)$ . For a one-dimensional disturbance (3.9-10) become:

$$\Delta \rho g \delta^2 / 2 + 2 \delta \tau_{xx} = F(t) \quad (B.1)$$

$$D\delta/Dt \equiv \delta_t + u\delta_x = -\delta u_x \quad (B.2)$$

where  $\tau_{ij}$  is the deviatoric stress tensor.

Below, we consider the particular case of a fluid with a power-law rheology. In mantle convection, the oceanic lithosphere makes up most of the cold, stiff upper thermal boundary layer. The lithosphere behaves like a rigid plate rather than a viscous fluid layer, so the results for a Newtonian fluid may be a poor model for destabilization of the lithosphere and the initiation of subduction. A better model might be a fluid where the stress depends on some power of the strain rate. This will not accurately describe fracturing, but can at least incorporate weakening at high rates of strain.

For a power-law fluid in quasi-one-dimensional flow:

$$\tau_{xx} = \mu_r |u_x|^n \quad (B.3)$$

where  $\mu_r$  has the appropriate units. Combining (B.1-3) we get a single

(dimensionless) Lagrangian equation describing the evolution of the thickness of the layer as we follow a material cross section:

$$D\tilde{\delta}/D\tilde{t} = \text{sgn}(\tilde{\delta} - \tilde{d}_e(\tilde{t})) \tilde{\delta} [|\tilde{\delta}^2 - \tilde{d}_e^2(\tilde{t})|/\tilde{\delta}]^m \quad (\text{B.4})$$

where  $m \equiv 1/n$ ,  $\tilde{\delta} \equiv \delta/h$ ,  $\tilde{t} \equiv (\Delta\rho gh/8\mu_r)^m t$ , and  $\tilde{d}_e(\tilde{t})$  is the nondimensionalized current equilibrium thickness as before. For the special case of a Newtonian fluid ( $n = m = 1$ ) this reduces to (3.10). When  $\tilde{d}_e(\tilde{t})$  is specified, (B.4) can be integrated numerically from the initial thickness  $\delta_0(x_0)$ . (Now drop tildes.)

For an infinitely long layer with a localized disturbance (i.e., constant end forces:  $d_e = 1$ ) and  $m$  an odd integer:

$$D\delta/Dt = (\delta^2 - 1)^m / \delta^{m-1} \quad (\text{B.5})$$

This can be integrated by parts. For example, if  $m = 3$ :

$$\tau(\delta) = 1/4 [ \delta/(\delta^2 - 1)^2 + 1/2 [ \delta/(\delta^2 - 1) + 1/2 \ln |(\delta - 1)/(\delta + 1)| ] ] \quad (\text{B.6})$$

where  $\tau(\delta) \equiv t_* - t$  is the time remaining before the thickness of the fluid cross section goes to  $\infty$  or 0. Profiles  $(\delta(x))$  for various  $t$  are shown in figure 8 for  $m = 3$  and  $m = 9$ , from an initial sinusoidal disturbance, using solutions of the above form.

The effect of increasing  $m$  is seen to be concentration of the deformation into narrow regions at the centers of peaks and troughs, while elsewhere the profile becomes linear in  $x$ . The growth remains slow initially, then suddenly becomes catastrophic after a certain threshold has been reached. A trough reaches this threshold and necks off much sooner than a peak of equal initial amplitude blows up. This can be seen in figure 9, which shows the growth of positive and negative perturbations over time.

When the amplitude  $a \equiv \delta - 1$  is small, the approximate solution is:

$$a \approx a_0 / [1 - (m-1)(2a_0)^{m-1}t]^{1/(m-1)} \quad (\text{B.7})$$

where  $a_0$  is the initial amplitude. This slow growth lasts for a period of roughly  $\Delta t \sim 1/[(m-1)(2a_0)^{m-1}]$ . For large amplitudes, the growth again becomes algebraic in the time remaining before the singularity is reached at  $t = t_*$ :

$$\delta_0 > 1: \quad \delta \approx 1/(m(t_*-t)) \quad (\text{B.8a})$$

$$\delta_0 < 1: \quad \delta \approx m(t_*-t) \quad (\text{B.8b})$$

This catastrophic growth occurs over a time scale  $\Delta t \sim 1/m$  (dimensionally  $(8\mu_r/\Delta\rho gh)^m/m$ ).

As for the Newtonian fluid, a disturbed region under constant end forces will tend to stretch out to some extent in the  $x$  direction. To keep the wavelength constant, the end forces must vary in time to give:

$$\int_0^L [(\delta^2 - d_e^2(t))/\delta]^m \delta \, dx = 0 \quad (\text{B.9})$$

While we have not done a numerical calculation for this case, we speculate that enforcing constant wavelength does not significantly alter the qualitative behavior, except to inhibit the layer from necking off. (When a fluid cross section reaches zero thickness, locally the strain must become infinite; for smooth initial conditions, this is incompatible with constant overall strain.) Also, peak growth may be slightly enhanced.

The main point is that when peaks get large (compared to the current equilibrium thickness), the large-amplitude effects still produce catastrophic growth of the form  $\delta \propto 1/(t_*-t)$ , as for a Newtonian fluid, where  $t_*-t$  is the time remaining before the singularity.

### C. LARGE-AMPLITUDE SIMILARITY SOLUTION

The equations appropriate to large-amplitude disturbances admit a rich family of similarity solutions, which illustrate a variety of behaviors. While such solutions demand particular initial conditions, nonetheless these

solutions can be interpreted as good local approximations for situations arising from arbitrary initial conditions. Two cases are of particular interest, in light of section 5: one describes how a smooth finite peak evolves to an infinite singularity, the other describes how that first singularity changes shape as the plume evolves.

Where  $\delta \gg d_e$  (in dimensionless terms), we can effectively set  $d_e = 0$  to get the large-amplitude equations, valid locally. In fact, the same equations would apply everywhere if somewhere the layer has zero thickness; for the case of constant end forces, minima in the layer (if initially less than  $d_e$ ) reach zero thickness in finite time. Then:

$$\delta_t + (u\delta)_x = 0 \quad (C.1a)$$

$$\delta + u_x = 0 \quad (C.1b)$$

We assume a similarity solution of the following form:

$$x = a(t)\xi, \quad \delta = A(t)f(\xi), \quad u = a(t)A(t)g(\xi) \quad (C.2)$$

Then the system (C.1) becomes:

$$(A'/A^2)f - (a'/(aA))\xi f' + (fg)' = 0 \quad (C.3a)$$

$$f + g' = 0 \quad (C.3b)$$

Similarity then requires that  $A'/A^2$  be a constant. If that constant is not zero we can normalize it by choosing the scale of  $A$ , and by a suitable choice of time origin:

$$A(t) = 1/t \quad (C.4a)$$

Then, because  $\delta$  must be non-negative, solutions where  $f > 0$  will apply for  $t > 0$ , when  $A$  is decreasing, and where  $f < 0$  will apply for  $t < 0$ , when  $A$  is increasing catastrophically to  $t = 0$ .

Also,  $a'/(aA)$  must be constant, say  $\lambda$ . (As  $\lambda$  is insensitive to the scale of  $a(t)$ , it cannot be normalized.) Then let:

$$a(t) = |t|^\lambda \quad (\text{C.4b})$$

For  $t > 0$ , positive  $\lambda$  gives a profile that spreads out in the  $x$  direction, while for negative  $\lambda$  the profile contracts; the converse is true for  $t < 0$ .

Combining (C.3a,b):

$$(gg')' - \lambda \xi g'' - g' = 0 \quad (\text{C.5})$$

which integrates to:

$$(g - \lambda \xi)g' + (\lambda - 1)g = C \quad (\text{C.6})$$

where  $C$  is an arbitrary constant. By a translation, corresponding to moving the origin to a different part of the layer moving at a different speed, the constant can be removed:

$$\zeta \equiv \xi - C/(\lambda^2 - \lambda), \quad q(\zeta) \equiv g(\xi) - C/(\lambda - 1) \quad (\text{C.7a})$$

$$(q - \lambda \zeta)q' + (\lambda - 1)q = 0 \quad (\text{C.7b})$$

as long as  $\lambda \neq 0, 1$ . Then the equation becomes separable for:

$$Q(\zeta) \equiv \zeta q(\zeta)$$

$$(Q - \lambda)\zeta Q' + (Q - 1)Q = 0 \quad (\text{C.8})$$

Integrating by partial fractions and substituting back gives:

$$\zeta = q + \text{sgn}(\zeta - q)D|q|^k \quad (\text{C.9a})$$

$$f = -1/[1 + \text{sgn}(q(\zeta - q))kD|q|^{k-1}] \quad (\text{C.9b})$$

where  $k \equiv \lambda/(\lambda - 1)$  and  $D > 0$  is the second arbitrary constant of integration.

This is the general solution; though the differential equation is nonlinear, a phase-plane analysis verifies that this gives all solutions (for  $A(t)$  not constant,  $\lambda \neq 0, 1$ ) except the trivial solutions  $f = 0$  and  $f = -1$ .

The solution describes a variety of behaviors, depending primarily on  $\lambda$  and on which branch of the solution is chosen. The constants  $C$  and  $D$  affect the  $x$  origin and scale, respectively.

For example, consider  $\lambda > 1$  (so  $k > 1$ ),  $C = 0$ ,  $D = 1$ , and the particular branch:

$$\xi = g + \text{sgn}(g)|g|^k \quad (\text{C.10a})$$

$$f = -1/[1 + k|g|^{k-1}] \quad (\text{C.10b})$$

Since  $f < 0$ , this solution only applies for  $t < 0$ ; it describes the growth of a peak up to the singular time when  $\delta$  at the peak becomes infinite. The asymptotics in  $\xi$  reveal the behavior:

$$\text{as } |\xi| \rightarrow 0: \delta \rightarrow |t|^{-1}[1 - k|t|^{-k}|x|^{k-1}], u \rightarrow -x/|t| \quad (\text{C.10c})$$

$$\text{as } |\xi| \rightarrow \infty: \delta \rightarrow |x|^{-1/\lambda/k}, u \rightarrow -\text{sgn}(x)|x|^{1/k} \quad (\text{C.10d})$$

The first (C.10c) applies for  $x$  near the origin, as long as  $t$  is non-zero. The peak is of fairly general shape, but for the peak to be analytic in  $x$ ,  $\lambda$  must be  $3/2$  ( $k = 3$ ). The second (C.10d) applies far from the origin early on ( $t \ll 0$ ), but applies ever nearer until at the singular time, it applies for all  $x$  ( $\neq 0$ ). The asymptotic shape (C.10d) is independent of time; as the peak grows it fills in the integrable negative power of  $x$  shape. For a smooth peak,  $\lambda = 3/2$  and at the singular time  $\delta \propto |x|^{-2/3}$  (for any  $D$ ).

As another example,  $\lambda > 1$ ,  $C = \text{sgn}(\xi)$ ,  $D = (\lambda-1)^k/\lambda$ , and the branch:

$$\xi = g - \text{sgn}(g)\lambda^{-1}[((\lambda-1)|g| + 1)^k - 1] \quad (\text{C.11a})$$

$$f = 1/[((\lambda-1)|g| + 1)^{k-1} - 1] \quad (\text{C.11b})$$

which describes a plume, symmetric in  $x$ , for  $t > 0$ . Asymptotically:

$$\text{as } |\xi| \rightarrow 0: \delta \rightarrow 1/[t^{1-\lambda/2}\sqrt{2|x|}], u \rightarrow -\text{sgn}(x)\sqrt{2|x|}/t^{1-\lambda/2} \quad (\text{C.11c})$$

$$\text{as } |\xi| \rightarrow \infty: \delta \rightarrow (\lambda|x|)^{-1/\lambda}, u \rightarrow -\text{sgn}(x)(\lambda|x|)^{1/k}/(\lambda-1) \quad (\text{C.11d})$$

At the singular time ( $t = 0$ ), the profile (C.11d), which is independent of time, applies everywhere. In other words, this example shows what happens to an initial profile proportional to an integrable negative power of  $x$ ; by a different choice of  $C$  and  $D$ , the profile (C.11d) could be made to match

(C.10d) exactly. For  $t > 0$ , (C.11c) applies near the origin; regardless of the starting  $x$  dependence, the shape around the singularity (plume) becomes proportional to  $1/\sqrt{|x|}$ . If  $\lambda < 2$  then the square-root singularity and the corresponding strength of the sink at the origin decay with time, as the layer drains away. (This would be true for an initially smooth profile like (C.10c) with  $\lambda = 3/2$ .) Conversely, for  $\lambda > 2$ , the singularity grows, as fluid comes in from the sides faster than it can be disposed of. The special case  $\lambda = 2$  gives a steady plume:

$$\delta = 1/\sqrt{2|x|}, \quad u = -\text{sgn}(x)\sqrt{2|x|} \quad (\text{C.11e})$$

Also, there are related solutions for  $\lambda = 0$ ,  $0 < \lambda < 1$ , and  $\lambda = 1$ , which have the same asymptotic shapes (C.11c,d), except that, for  $|\xi| \rightarrow \infty$ , the forms for  $u$  are different, and for  $\lambda = 0$ ,  $\delta \rightarrow e^{-|x|}/t$  as  $|\xi| \rightarrow \infty$ .

Briefly, the other behaviors governed by the similarity solution are as follows. For  $t < 0$ , i.e., profiles growing to the singular time, there are four: a minimum thickness of zero like  $|x|^k$ ,  $k > 0$ , locally time-independent, that far away levels off to approach  $1/|t|$ ; a profile that approaches zero as  $x \rightarrow -\infty$  and  $1/|t|$  as  $x \rightarrow +\infty$ ; a symmetric finite minimum flanked by plumes (which could be extended periodically); and a plume whose sides level off to approach  $1/|t|$  (rather than 0). For  $t > 0$ , where the profile starts at the singular time and diminishes thereafter, there is only one other case: a zero minimum flanked by plumes (which could extend periodically). The special case of  $A(t) = 1$ , so  $a(t) = e^{\lambda t}$ , gives either an isolated plume, or a zero minimum where  $|\delta_x| \rightarrow \infty$  surrounded by plumes (possibly periodic). All cases with plumes show the  $1/\sqrt{|x|}$  shape. And solutions with the same  $A(t)$  and  $\lambda$  but different  $C$  and  $D$  can be "cut and pasted" together to give other similarity profiles: if  $g$  and  $g'$  are continuous this will produce reasonable results.



REFERENCES

- Canright, D. R., 1987. A finite-amplitude analysis of the buoyant instability of a highly viscous film over a less viscous half-space. Ph.D. thesis, University of California, Berkeley, California.
- Whitehead, J. A., and Luther, D. S., 1975. Dynamics of laboratory diapir and plume models. J. Geophys. Res. 80, #5: 705-717.

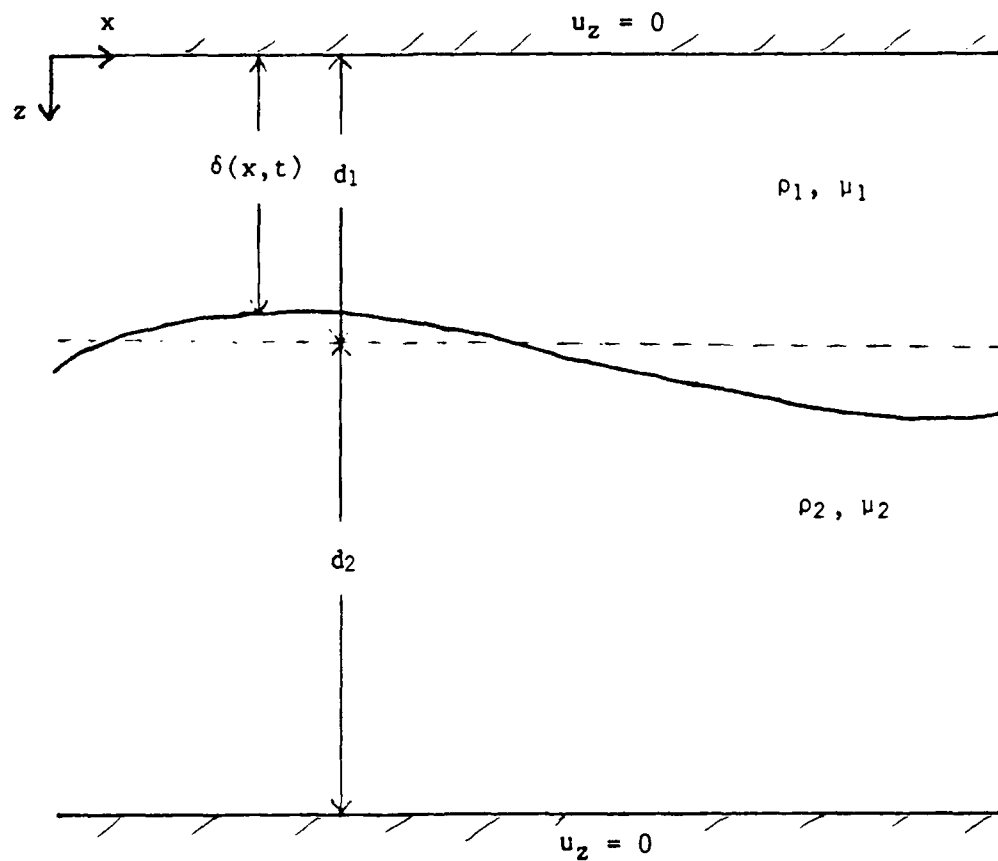


Figure 1. Rayleigh-Taylor Problem. A layer of fluid 1 over a layer of a different fluid 2, between shear-free boundaries, where  $\rho_2 < \rho_1$ . Interface position given by  $z = \delta(x, t)$ . Equilibrium (unstable) depths of upper and lower layers are  $d_1$  and  $d_2$ . Growth rate of instability depends on viscosity ratio  $\alpha \equiv \mu_1/\mu_2$ , thickness ratio  $\beta \equiv d_1/d_2$ , and wavenumber  $k$  (dimensionless  $\epsilon \equiv kd_1$ ).

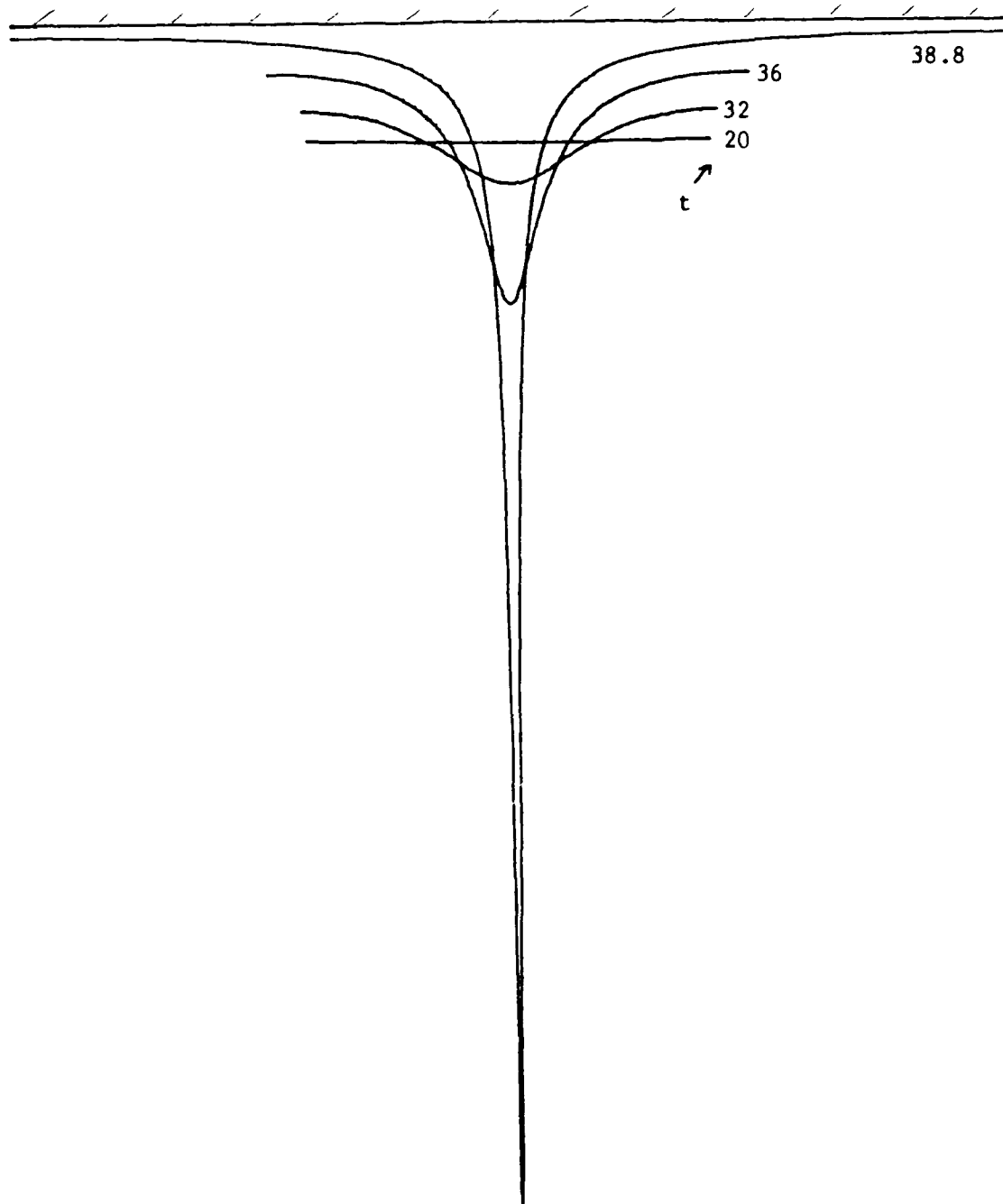


Figure 2. Viscous Layer Profiles  $\delta(x)$  for various times  $t$ , from initial sinusoidal perturbation of amplitude  $10^{-4}$ , for constant end-force conditions ( $d_e = 1$ ). Each profile represents one wavelength; the overall strain increases with time.

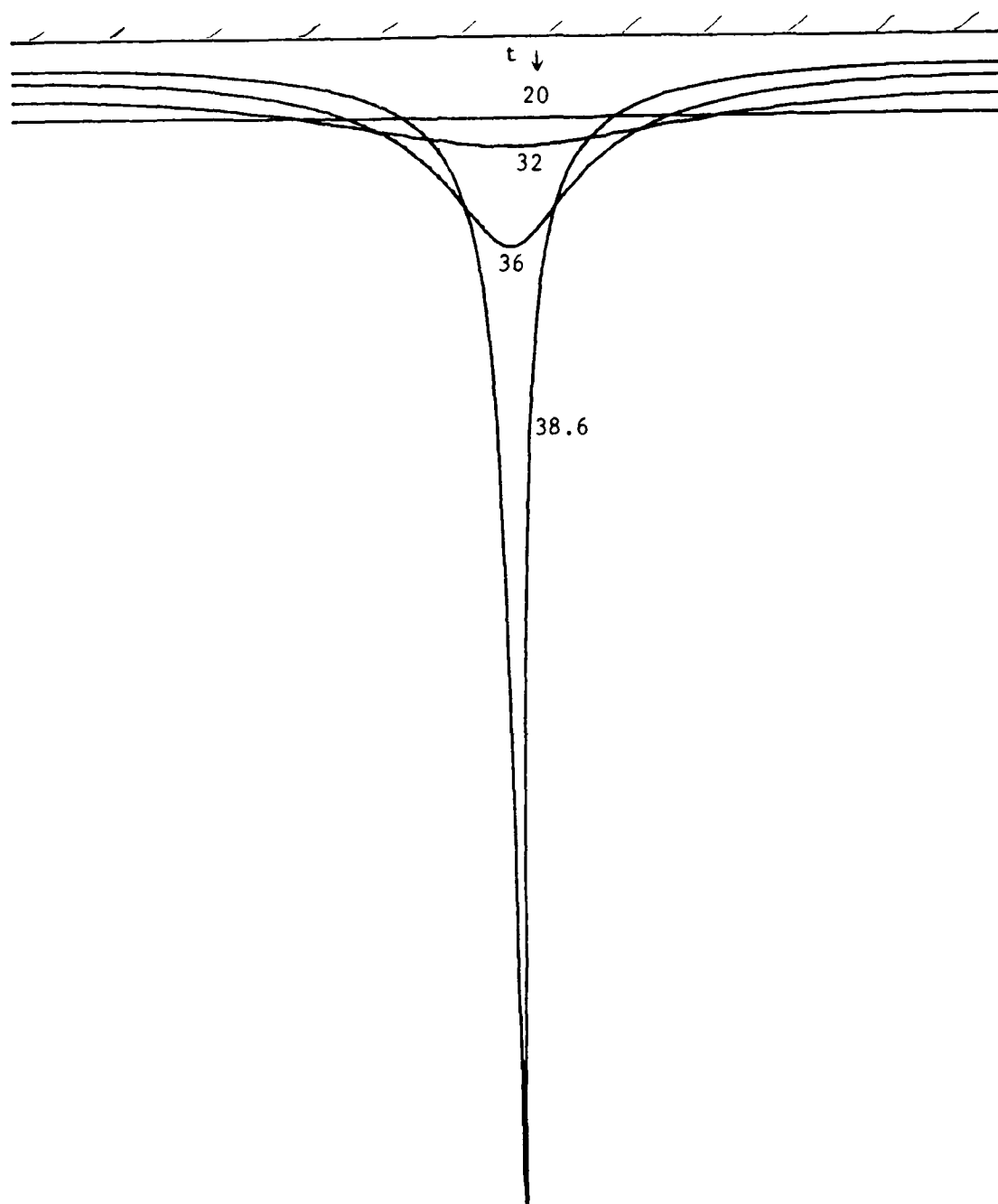


Figure 3. Viscous Layer Profiles  $\delta(x)$  for various times  $t$ , from initial sinusoidal perturbation of amplitude  $10^{-4}$ , for constant wavelength conditions ( $d_e(t)$  decreases with time). Similar to Fig. 2, except troughs not as deep, and the peak reaches  $\infty$  slightly sooner.

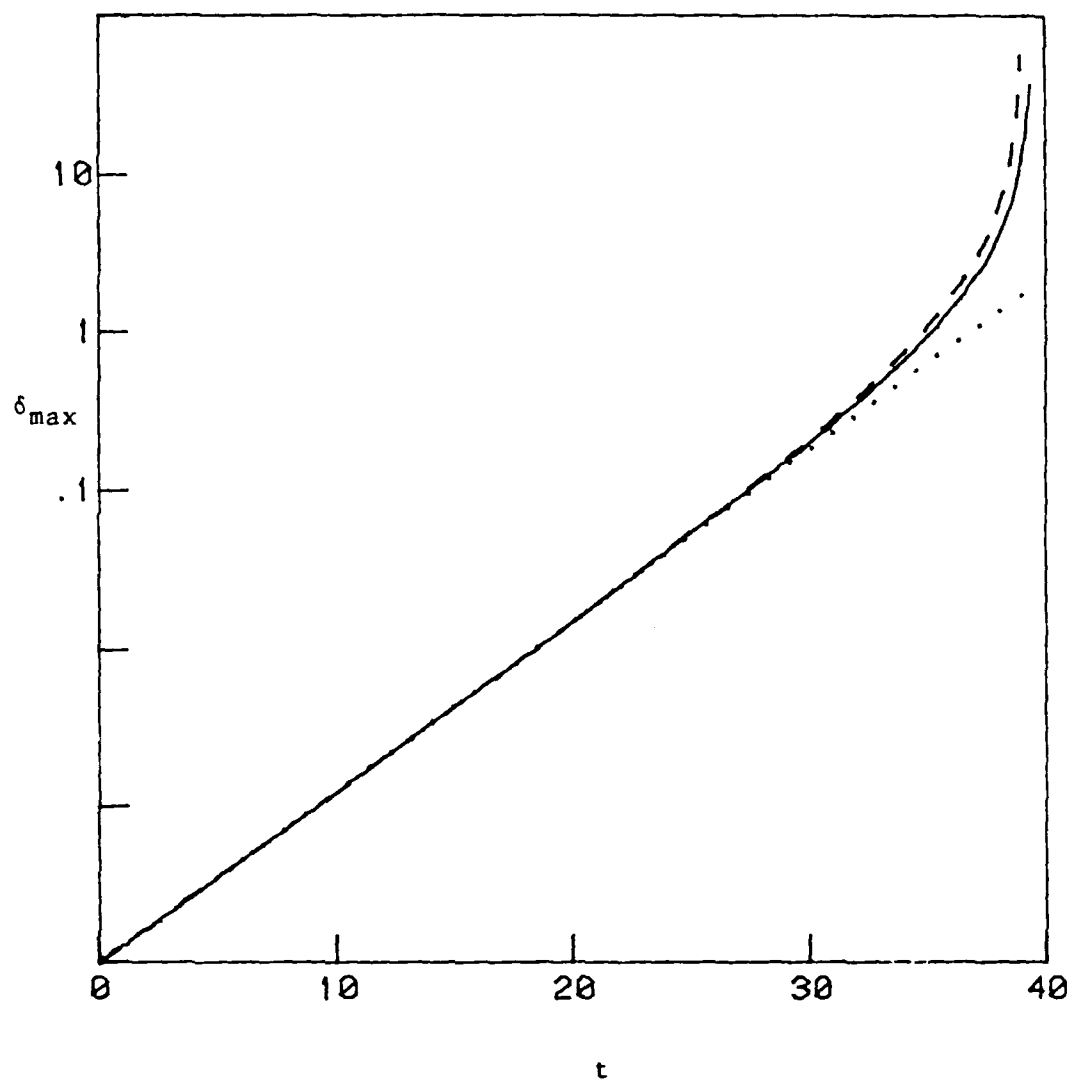


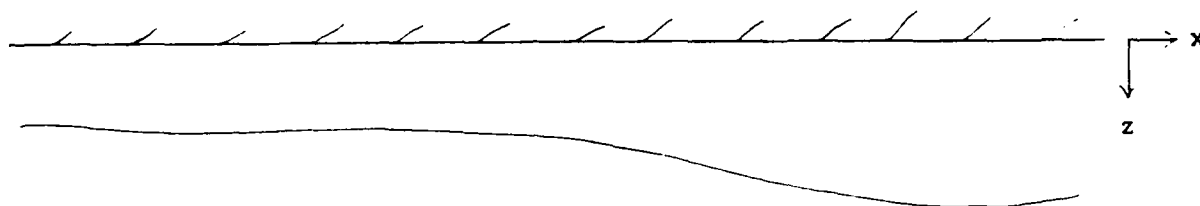
Figure 4. Peak Disturbance Growth:  $\delta_{\max}(t)-1$  (logarithmic) vs. time, from initial sinusoidal perturbation of amplitude  $10^{-4}$ .

(solid): for constant end force

(dashed): for constant wavelength

(dotted): exponential (linearized) growth, for comparison

$t = 0$



$t = t_*$

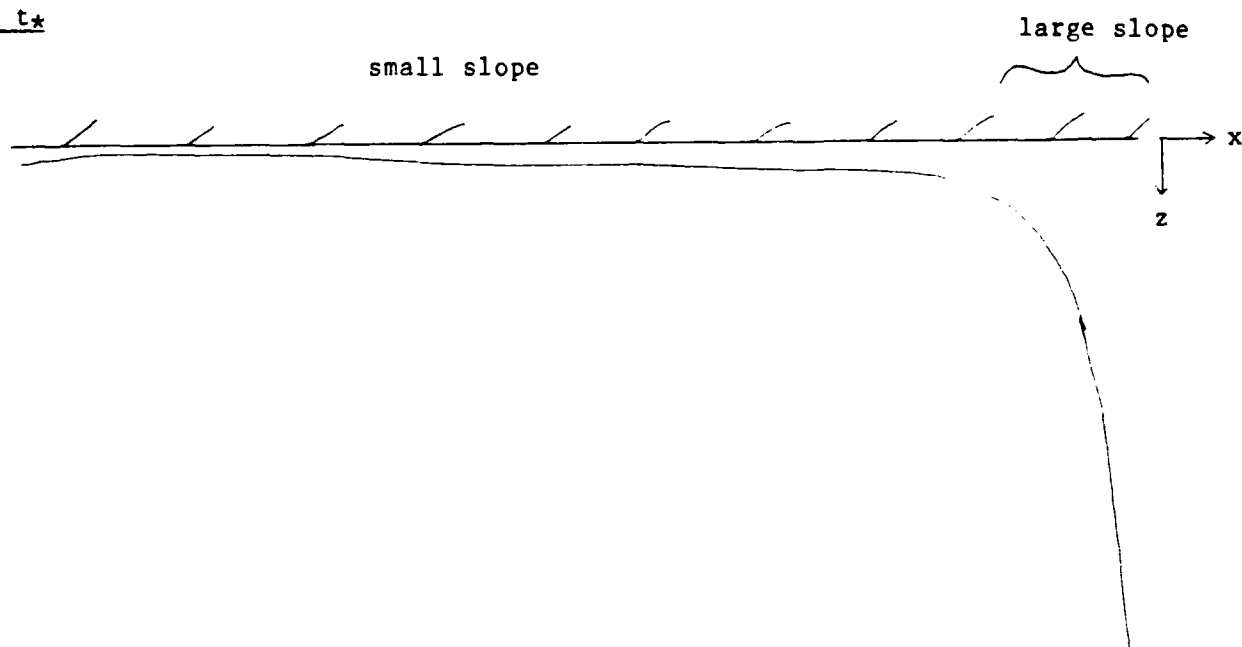


Figure 5. When small-slope approximation fails, it does so only in a region of width  $O(\epsilon)$ .

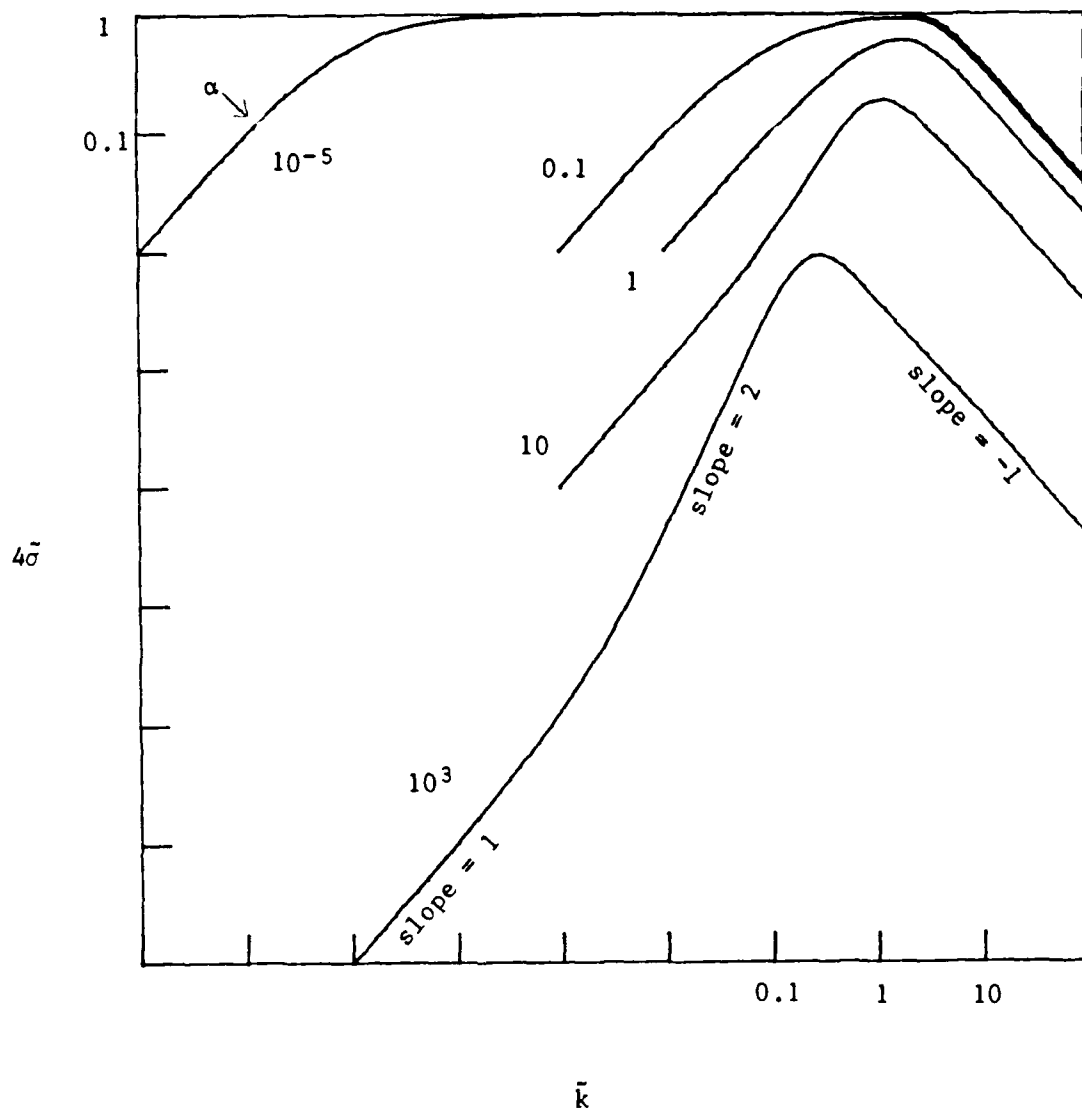


Figure 6a. Linearized Growth Rate:  $\tilde{\sigma}(\tilde{k})$  (logarithmic scales)  
 (a) Infinite depth ( $\beta \rightarrow \infty$ ), for various viscosity ratios  $\alpha$ . This shows that when the film is much more viscous than the fluid below ( $\alpha \ll 1$ ), the maximum growth rate applies over a broad range of wavelengths (to lowest order).

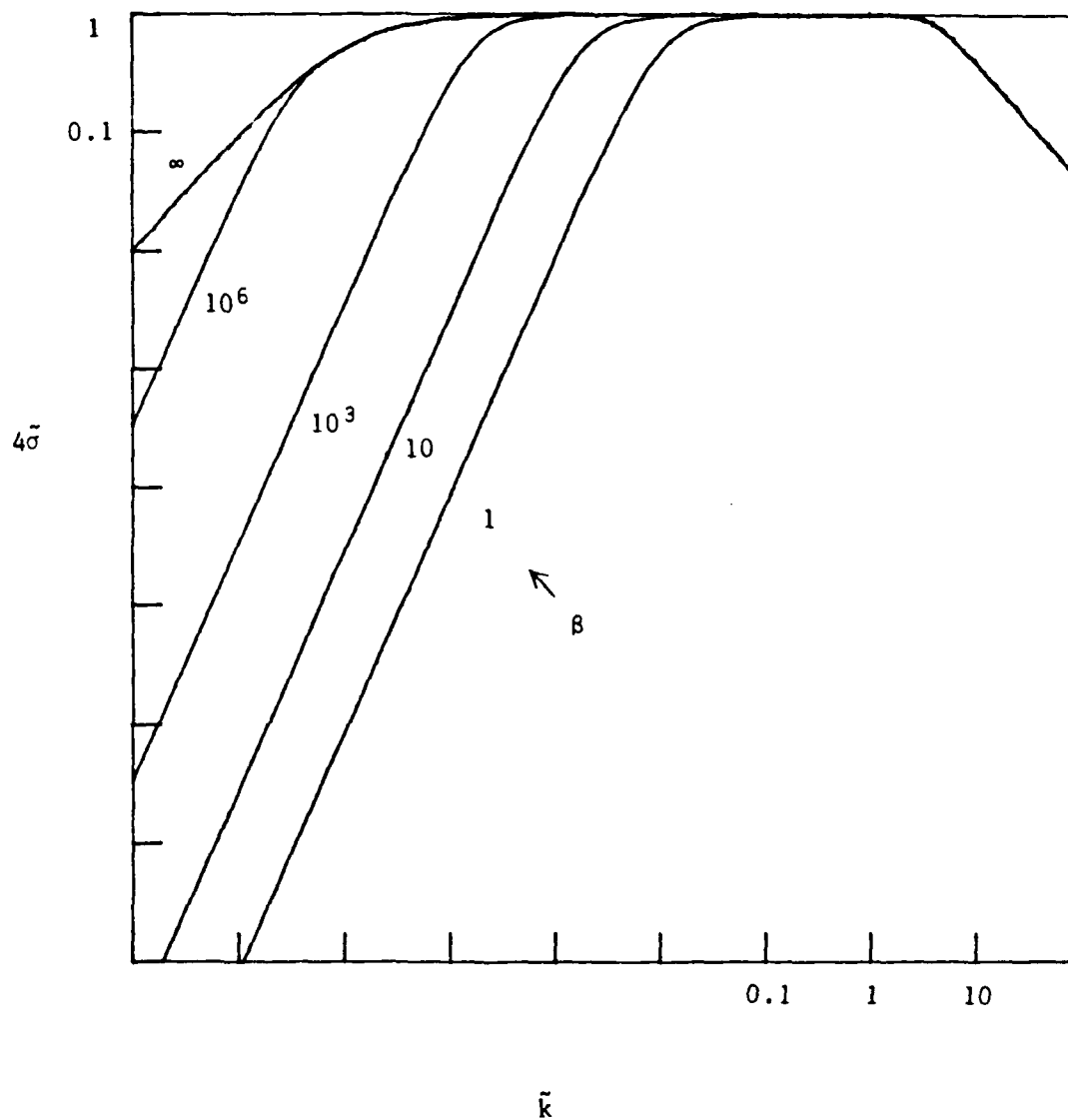


Figure 6b. Linearized Growth Rate:  $\tilde{\sigma}(\tilde{k})$  (logarithmic scales)  
 (b) Finite depth (various  $\beta$ ), for  $\alpha = 10^{-5}$ . This shows how finite-depth effects give a large-wavelength cutoff to the maximum growth regime for  $\alpha \ll 1$ .



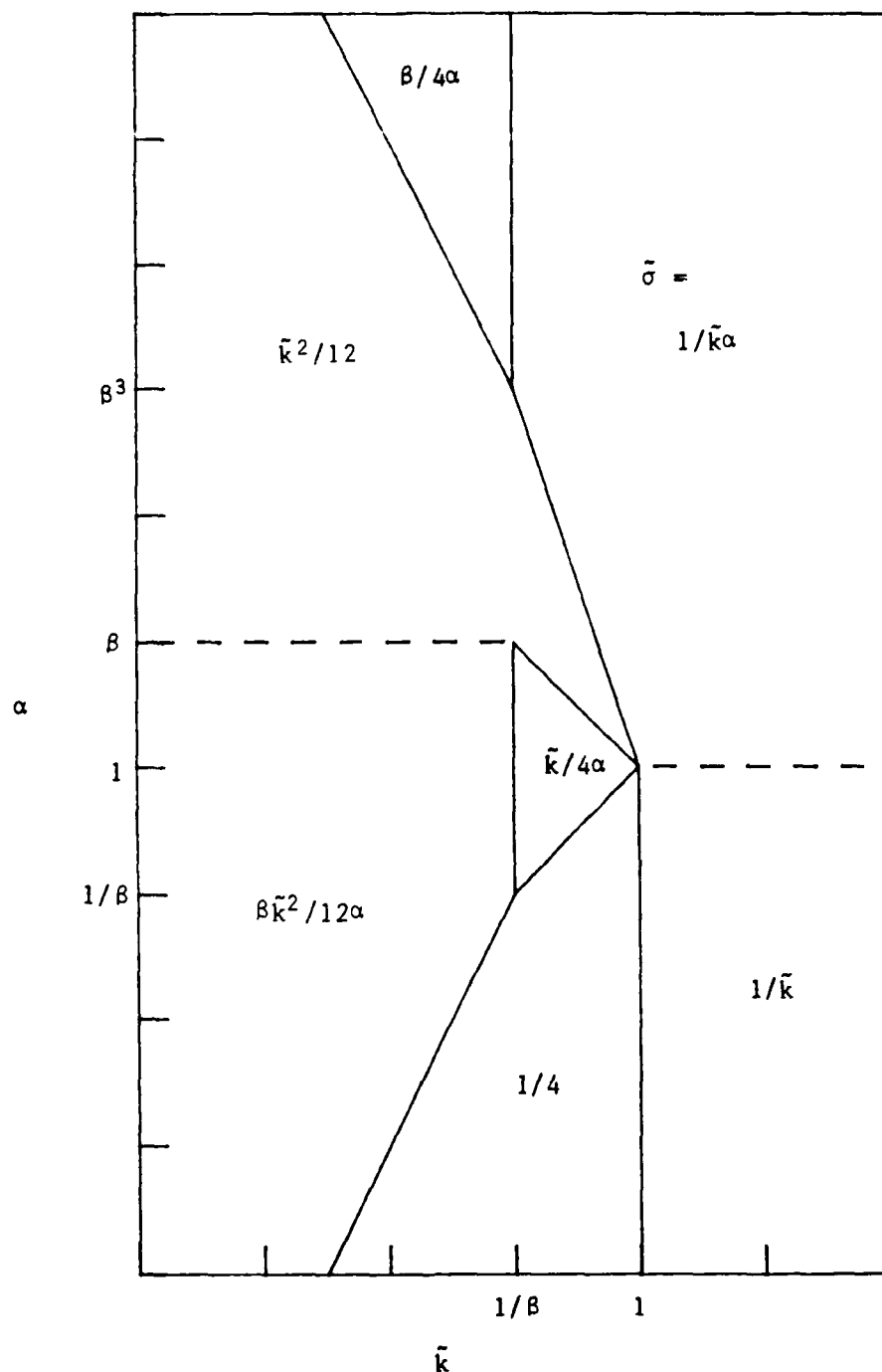


Figure 7. Rayleigh-Taylor Growth Regimes. The various (dimensionless) asymptotic growth rates  $\bar{\sigma}$  (from Eq. A.3c) are shown in the regions of the parameter plane (wavenumber  $\bar{k}$  and viscosity ratio  $\alpha$ , logarithmic scales) where they apply, assuming the depth ratio  $\beta \gg 1$ . (Divisions between regions, shown as lines, are actually broad areas across which the growth rate varies continuously.) These growth regimes apply while the interface slope remains small, which for long waves ( $\bar{k} \ll 1$ ) includes large amplitudes.

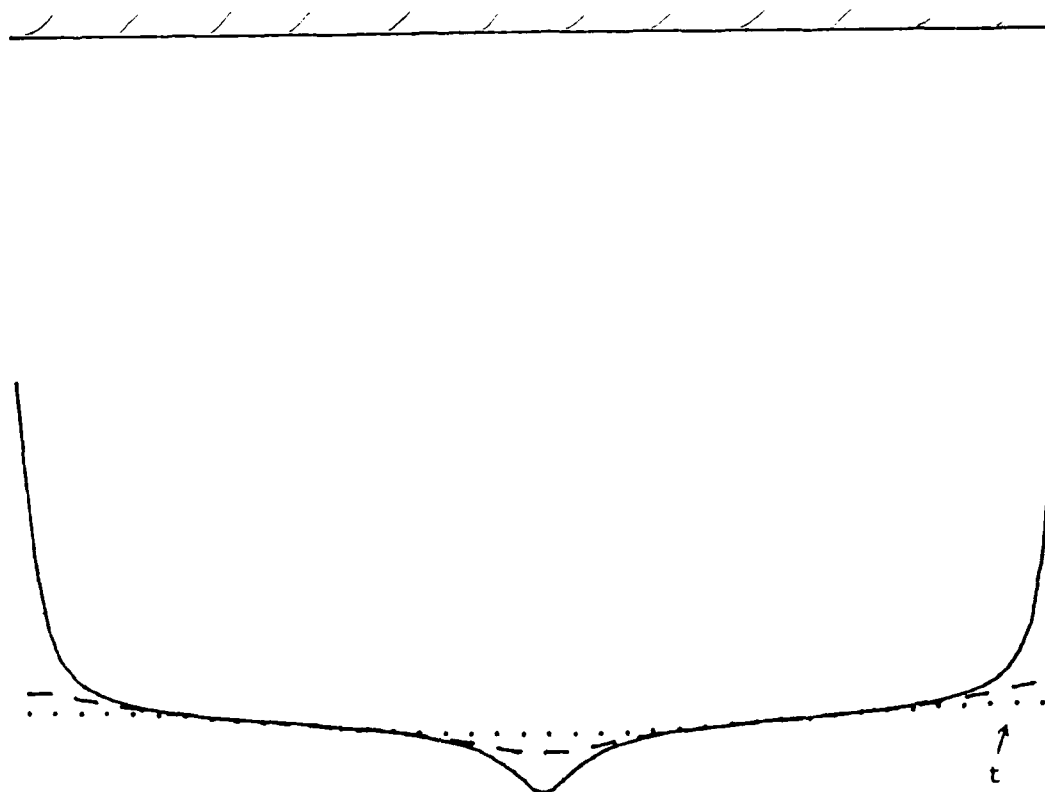


Figure 8a. Power-Law Fluid Layer Profiles:  $\delta(x)$  for various times  $t$ , from an initial sinusoidal perturbation of amplitude 0.02, assuming constant end-force conditions.

- (a) for power  $m = 3$ 
  - (dotted): initial,  $t = 0$
  - (dashed):  $t = 129$
  - (solid):  $t = 153$

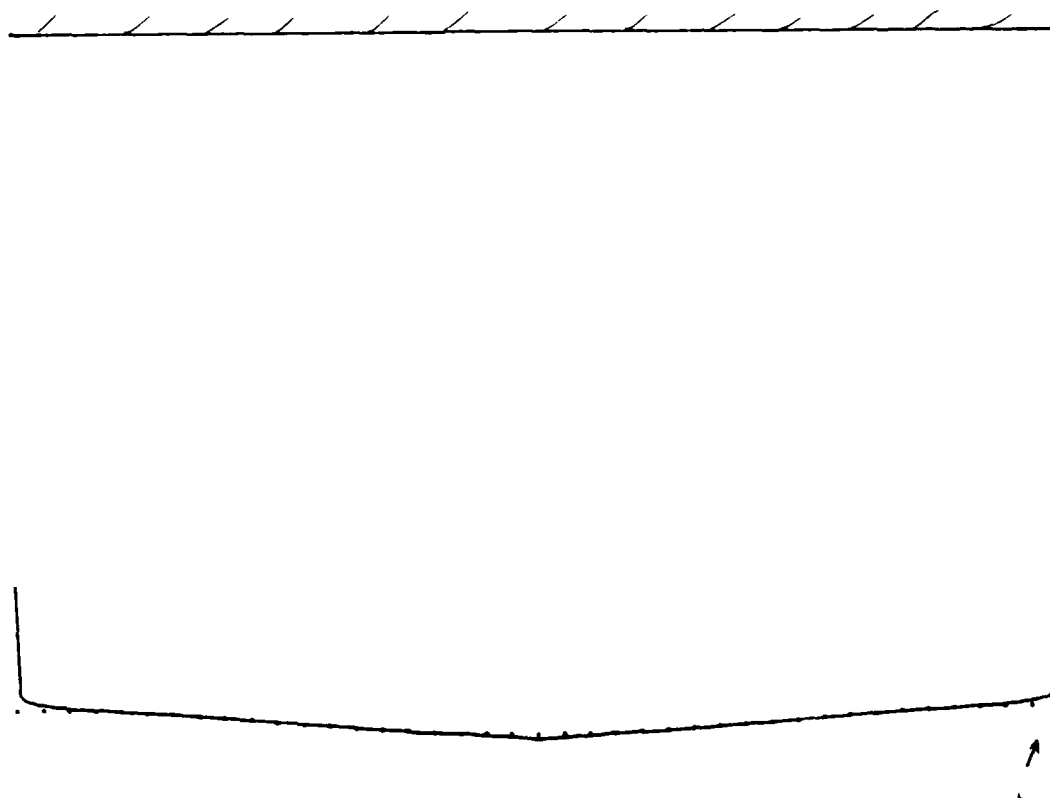


Figure 8b. Power-Law Fluid Layer Profiles:  $\delta(x)$  for various times  $t$ , from an initial sinusoidal perturbation of amplitude 0.02, assuming constant end-force conditions.

- (b) for power  $m = 9$
- (dotted): initial,  $t = 0$
- (solid):  $t = 8.8 \times 10^9$

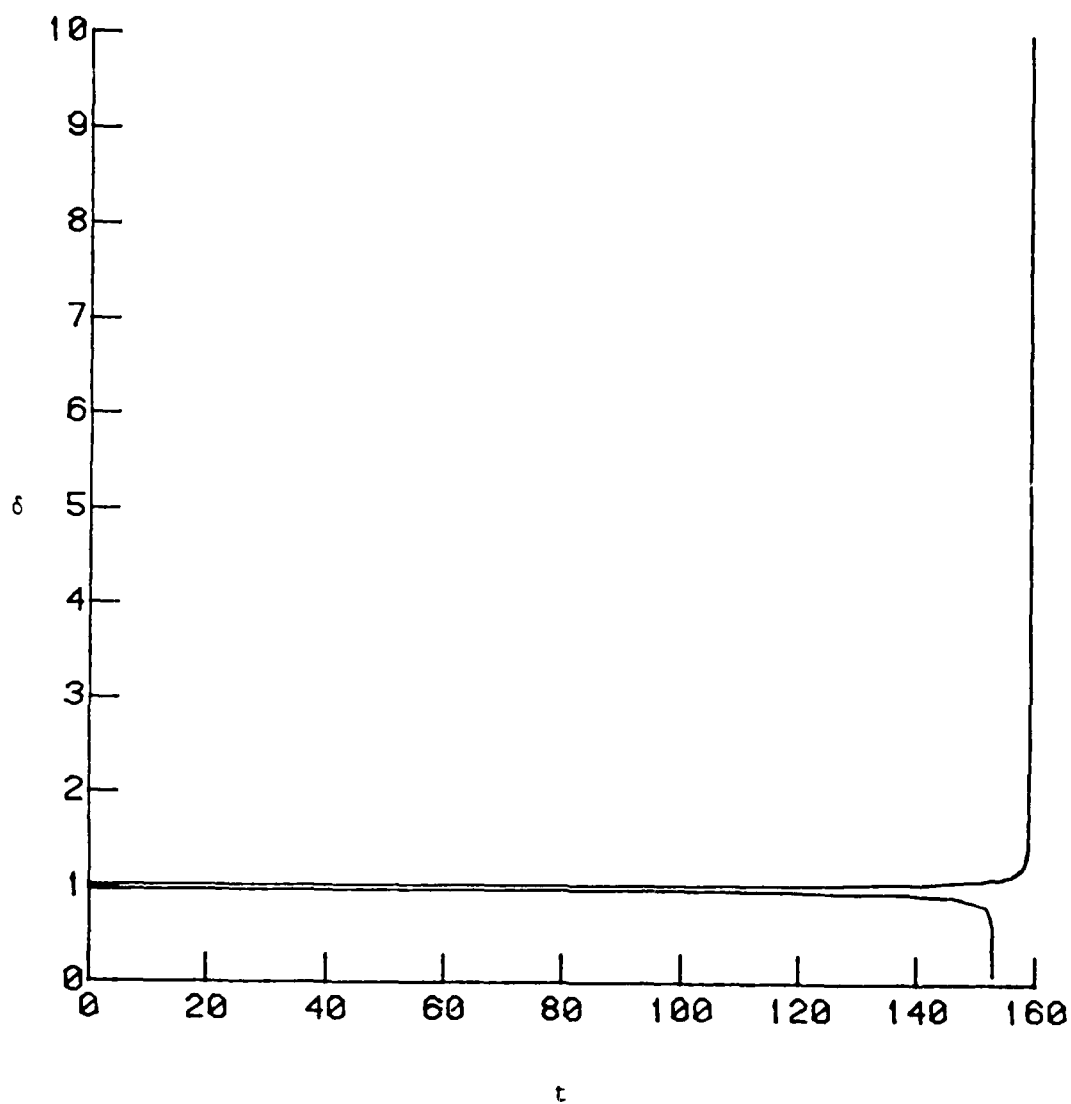


Figure 9a. Power-Law Fluid Disturbance Growth:  $\delta(t)$  (linear scales) following a fluid cross section, from an initial perturbation amplitude of 0.02, assuming constant end forces. Growth is shown for both positive and negative perturbations.  
 (a) for power  $m = 3$

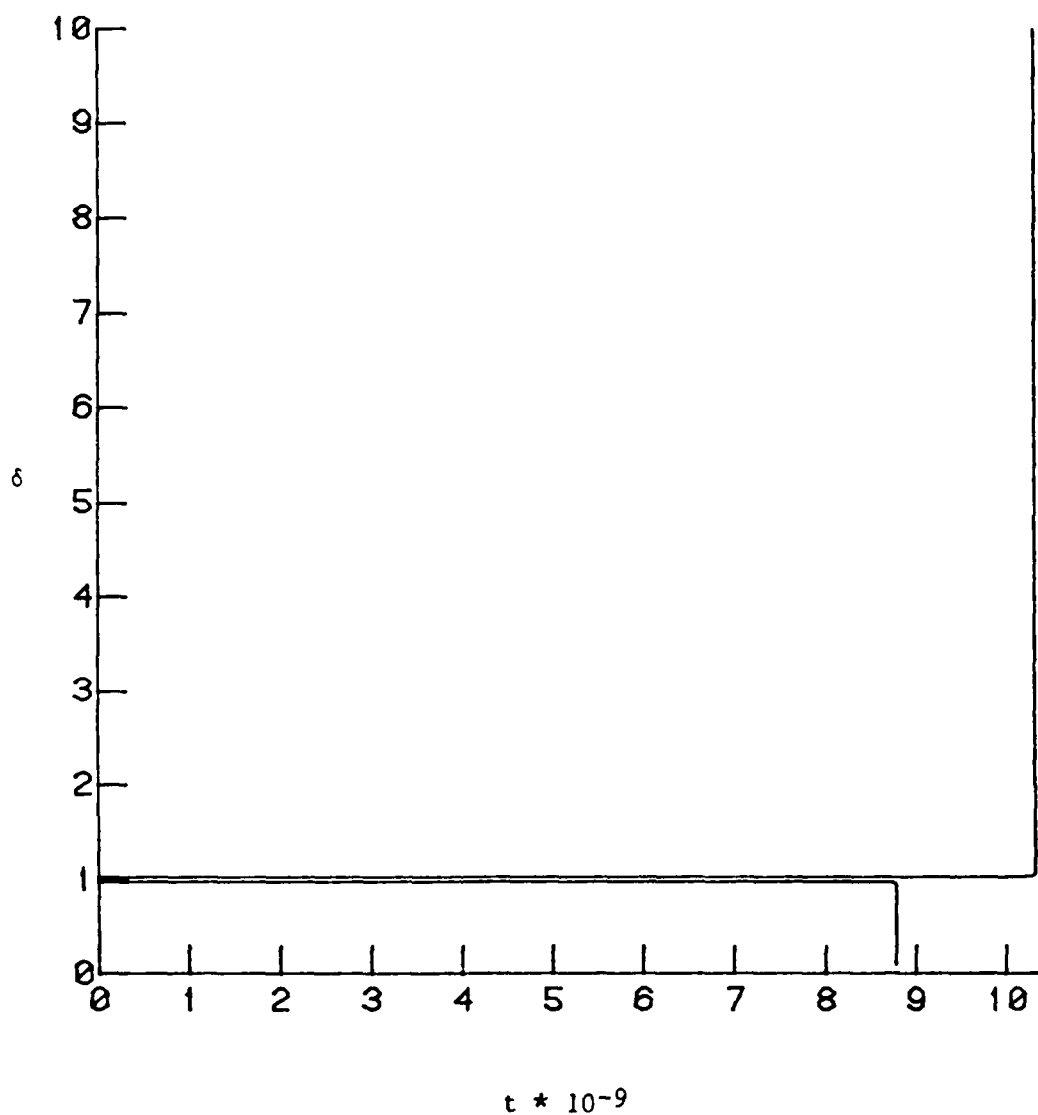


Figure 9b. Power-Law Fluid Disturbance Growth:  $\delta(t)$  (linear scales) following a fluid cross section, from an initial perturbation amplitude of 0.02, assuming constant end forces. Growth is shown for both positive and negative perturbations.  
 (b) for power  $m = 9$

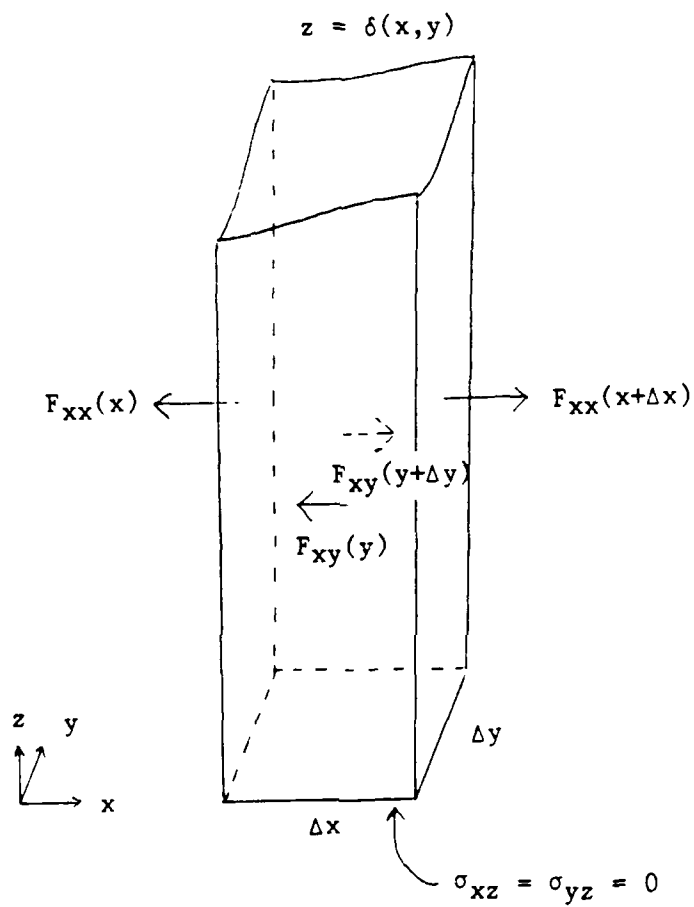


Figure 10. Force balance on a differential column of fluid ( $z$  upward).

DISTRIBUTION LIST

DIRECTOR  
DEFENSE TECH. INFORMATION CENTER (2)  
CAMERON STATION  
ALEXANDRIA, VA 22314

DIRECTOR OF RESEARCH ADMIN.  
CODE 012  
NAVAL POSTGRADUATE SCHOOL  
MONTEREY, CA 93943

LIBRARY (2)  
CODE 0142  
NAVAL POSTGRADUATE SCHOOL  
MONTEREY, CA 93943

DEPARTMENT OF MATHEMATICS  
CODE 53  
NAVAL POSTGRADUATE SCHOOL  
MONTEREY, CA 93943

CENTER FOR NAVAL ANALYSES  
4401 FORD AVENUE  
ALEXANDRIA, VA 22302-0268

ADJUNCT PROFESSOR DAVID CANRIGHT (15)  
CODE 53Ca  
DEPARTMENT OF MATHEMATICS  
NAVAL POSTGRADUATE SCHOOL  
MONTEREY, CA 93943

NATIONAL SCIENCE FOUNDATION  
WASHINGTON, D.C. 20550